Consideration of Low Viscous Droplet Breakage in the Framework of the Wide Energy Spectrum and the Multiple Fragments

Luchang Han, Shenggao Gong, Yaowen Ding, Jin Fu, Ningning Gao, and He'an Luo
Dept. of Chemical Engineering, School of Chemical Engineering, Xiangtan University, Hunan 411105, P.R. China

DOI 10.1002/aic.14830
Published online May 13, 2015 in Wiley Online Library (wileyonlinelibrary.com)

An improved model for low viscous droplet breakage has been developed. Unlike the previous work that considered the inertia subrange and adopted the assumption of binary breakage, this work considered the breakage of droplets in the framework of the multiple fragments and the wide energy spectrum (i.e., including the dissipation range, the inertia subrange, and the energy containing range simultaneously). The previous interactions between the droplet and the surrounding fluids have been considered through introducing the interaction forces. The effect of the surface deformation and oscillation resulting from these interactions on the constraints of multiple breakages has been accounted for. These factors have been neglected in the existing models. The wide energy spectrum distribution was found to have an important effect on the nonmonotone evolution of breakage frequency with increasing parent droplet size. The cumulative volume fractions predicted by this work showed a better agreement with the experimental data. © 2015 American Institute of Chemical Engineers *AIChE J*, 61: 2147–2168, 2015
Keywords: multiple breakages, daughter-size distribution, droplet, wide energy spectrum, turbulent flow

Introduction

The breakage of fluid particles widely exists in multiphase flow reactors or equipments, for example, mixing vessel, extraction column, and distillation tower. The breakage processes of fluid particles usually determine the size distribution of dispersed phase and interfacial area, and thus play a crucial role in mass transfer, heat transfer, and the design of chemical equipments. In past decades, many mathematical models for fluid particle breakage were proposed, please see the excellent reviews given by Lasheras et al.,[1] Jakobson,[2] Liao and Lucas,[3] Marchetti and Svendsen,[4] Solsvik et al.,[5] and Zainal Abidin et al.[6]

Previous work on breakage models

Coulaloglou and Tavlarides[7] defined the breakage frequency of parent fluid particle of size d_0 as a product of the fraction particles breaking and the reciprocal time needed for breakage. They obtained the total breakage frequency, that is, $b(d_0) = C_1\varepsilon^{1/3}d_0^{-2/3}\ \exp[-C_2\sigma/(\rho_d\varepsilon^{2/3}d_0^{5/3})]$. Here, C_1 and C_2 are empirical constants which need to be fitted from the experimental data, and the two parameters were taken as 0.336 and 0.106, respectively, in their original paper. This model exhibits a maximal breakage frequency when the parent fluid particle size d_0 increases. This nonmonotonic behavior was considered to be questionable by several investigators.[8,9] However, such a phenomenon has been observed by the recent experimental results.[10] Coulaloglou and Tavlarides[7] also proposed the daughter-size distribution (DSD) function for population balance equation (PBE) that is, $2.4\exp[-4.5(2V/V_0-1)^2]/V_0$.

Prince and Blanch[11] argued that the breakage frequency density $\Omega(d_0)$ can be written as the product of collision frequency of arriving eddies and breakage efficiency. The breakage efficiency can be viewed as the fraction of the eddies with the kinetic energy larger than or equal to the critical energy required for fluid particle breakage, that is, $\exp(-u_c^2/u_c^2)$. Where u_c was based on the critical Weber number, and denotes the critical eddy velocity required for breakage. The nonmonotonic behavior of the breakage frequency density with increasing d_0 can be exhibited by this model. Notice that $\Omega(d_0)$ was called breakage rate (denoted as β_i) in the original paper of Prince and Blanch,[11] but its unit seems different from $b(d_0)$ proposed by Coulaloglou and Tavlarides.[7] That is, the unit of $\Omega(d_0)$ is $1/(m^3\ s)$ while the unit of $b(d_0)$ is 1/s. Thus, $\Omega(d_0)$ is called breakage frequency density (or breakage density according to the suggestion given by Solsvik et al.[5]) in this work. In addition, the breakage frequency $b(d_0)$ can be obtained from $\Omega(d_0)/n_d$, n_d is the number of fluid particles per unit space volume.

Based on the relationship between surface restoring pressure and turbulence fluctuation pressure produced by surrounding fluid, Martínez-Bazán et al.[12] proposed a breakage frequency model for gas bubbles. They argued that gas bubbles could deform and break up when turbulent fluctuation pressure is larger than surface restoring pressure. The breakage frequency was proportional to the reciprocal of breakage time.

Correspondence concerning this article should be addressed to L. Han at happy-929@163.com or H. Luo at hluo@xtu.edu.cn.

The breakage frequency $b(d_0)$ could be expressed as $C_3\sqrt{\Delta u^2(d_0)-12\sigma/\rho_c d_0}/d_0$. Where C_3 is an empirical constant, and it was taken as 0.25 in their original paper. Martínez-Bazán et al.[12] assumed that the probability of forming a certain pair of daughter bubbles should be proportional to the product of excess stresses ($\Delta\tau=\beta_1\rho_c\ (\varepsilon d_0)^{2/3}/2-6\sigma/d_0$) corresponding to each daughter bubble size. Based on this assumption, a DSD function was proposed by them. They further proposed that bubble broke into one daughter bubble and other two identical daughter bubbles, and a model of DSD for ternary breakage was obtained Ref. 13.

Luo and Svendsen[14] defined the breakage frequency density $\Omega(d_0)$ as the product of the collision frequency and the breakage probability or efficiency. The breakage probability was obtained from the turbulent kinetic energy distribution and the critical energy criterion. They proposed that the kinetic energy of arriving eddies should be equal to or more than the increase of surface energy required for breakage (i.e., $e(\lambda)\geq c_f\pi d_0^2$, where $c_f=f_v^{2/3}+(1-f_v)^{2/3}-1$). Lehr and Mewes,[15] Lehr et al.,[16] Wang et al.,[17] Xing et al.,[18] and Zhao and Ge[19] also established the breakage frequency density model for bubbles. The breakage constraint in the model of Lehr and Mewes[15] and Lehr et al.[16] was based on the dynamic pressure criterion, which was obtained from the force balance (i.e., $\rho_c u_\lambda^2/2\geq c_0\sigma/d_1$, where c_0 is 1[15] or 2[16], d_1 is the size of smaller daughter fluid particle). Wang et al.[17] proposed the criterion of combining the dynamic pressure or capillary pressure and surface energy increase. In their model, $\rho_c u_\lambda^2/2\geq\sigma/d_1$ was used to determine $f_{v,\ \min}$, and $e(\lambda)\geq c_f\pi d_0^2$ was used to determine $f_{v,\max}$. They further assumed that f_v obeys a uniform distribution in ($f_{v,\min}$, $f_{v,\max}$). The recent work of Xing et al.[18] considered the mechanism of internal flow redistribution for bubble/droplet. Zhao and Ge[19] used the combining criterion, that is, $e(\lambda)\geq\max\left[c_f\pi d_0^2,\ (2\sigma/d_1)\pi\lambda^3/6\right]$.

The corresponding DSD functions have also been established by Luo and Svendsen,[14] Lehr and Mewes,[15] Lehr et al.,[16] Wang et al.,[17] Xing et al.,[18] and Zhao and Ge,[19] respectively. The DSD is U-shaped in the model of Luo and Svendsen.[14] The DSD given by the model of Luo and Svendsen[14] showed that the unequal-size breakage is most likely. Nevertheless, the probability density predicted by this model goes to infinite when the daughter-size fraction f_v tends to 0 or 1, this shortcoming was modified by Hagesaether et al.[20] The DSD given by the model of Lehr and Mewes[15] and Lehr et al.[16] exhibits a log-normal distribution, and the DSDs in both the models of Wang et al.[17] and Zhao and Ge[19] are M-shaped.

These above breakage models usually assumed that d_0 mainly falls in the inertia subrange and then the energy spectrum of inertia subrange (ESIS) was usually used to establish the breakage model. However, according to the turbulence theory, the width of inertia subrange usually depends on turbulent dissipation rate and physical properties of fluids. This indicates that it may not be assured that all the sizes of fluid particles always fall in this range in many actual situations. Therefore, the contribution of wide energy spectrum (i.e., including the energy containing range and the dissipation range) to the breakage of droplets needs to be considered.

Previous work on breakage experiments

In turbulent dispersions, the processes of fluid particle breakage are very complex. Therefore, the assumption of binary breakage was often introduced to simplify the breakage processes and establish the breakage model. However, the experiments of single droplet breakage[10,21,22] showed that more than two daughter droplets may be formed after a breakage. This phenomenon indicates that the multiple breakage processes may need to be considered for droplets. Several experimental works for droplets or bubbles breakage will be briefly reviewed here.

Konno et al.[23] used high-speed photography to observe droplet breakage events in stirred tank. The dispersed phase was a mixture of o-xylene and carbon tetrachloride, the continuous phase was distilled water. A small amount of Na_3PO_4 was added to distilled water to prevent adhesion of droplets to the wall of mixing apparatus. The fraction of dispersed phase was less than 0.2% in their experiments to avoid coalescence among droplets. The parent droplet size ranged from about 0.26–1.0 mm, and the mean number of daughter droplets mainly ranged from 2 to 4.

Martínez-Bazán et al.[12] performed bubble breakage experiments in a fully developed turbulent flow. The turbulent dissipation rate ε ranged from about 20.0–2800 $m^2\ s^{-3}$. The measured breakage frequencies exhibit an increase with increasing ε, and exhibit a decrease with increasing d_0 in the measured mean range of bubbles (i.e., about 1.67–2.75 mm). Eastwood et al.[24] extends the work of Martínez-Bazán et al.[12] to liquid–liquid system. Five different dispersed phases were used in their experiments to study the effect of viscosity of dispersed phase on droplet breakage. The experiments showed that the droplets were deformed or elongated first, and then formed a complex body before breakage.

In a relatively wide range of water flow velocities (i.e., $4300<\mathrm{Re}<10{,}600$), Galinat et al.[25] performed the experiments of single heptanes droplet breakage in turbulent pipe flow downstream of a restriction. The systems of heptane in water and dyed heptane in water were studied in their experiments. Galinat et al.[25] found that the mean number of daughter droplets after breakage mainly ranged from 2 to 4 when Weber number varied from about 20–40. Andersson and Andersson[21] performed the experiments of bubbles and droplets breakage in turbulent pipe flows. They found that the probability of binary breakage of bubbles is more than about 95%, while the binary, ternary, and quaternary breakages of low viscous droplets mainly occur when turbulent dissipation rate ranged from 3.7 to 16.3$m^2\ s^3$. The experiments showed that the droplets were considerably deformed and elongated before breakage.

Zaccone et al.[22] measured the DSDs for the breakages of forming two, three, and four daughter droplets, respectively, in a breakage cell. Maaβ and Kraume[10] measured the breakage frequency of single droplet (petroleum and toluene) in a breakage cell. Both of the devices in the experiments of Zaccone et al.[22] and Maaβ and Kraume[10] were used to represent the turbulent flow near the impeller blade. The multiple breakage processes of droplets were observed in their experiments through a high-speed camera. According to the pictures of the trajectory of droplet given by Maaβ and Kraume,[10] the process of ternary breakage of low viscous droplet could be decomposed as the following steps. The parent droplet was first deformed and stretched (i.e., became a very complex body), one daughter droplet was then split from the complex body, and then the residual part of the complex body broke into the second and third daughter droplets after a very short time. The similar process of ternary

breakage was also observed in the experiments of Galinat et al.[25] The experiments of Maaβ and Kraume[10] further showed that the breakage frequency increases to a maximum and then decreases with increasing d_0.

Purpose of this work

As seen from the above review, the assumption of binary breakage for droplets seems too simple since it cannot fully reflect the multiple breakage process. Furthermore, as mentioned before, the contribution of eddies to the breakage needs to be considered in the wide energy spectrum range (i.e., including the dissipation range, the inertia subrange and the energy containing range simultaneously) since it may not be assured that the sizes of droplets mainly fall in the inertia subrange. Finally, the evolution of the breakage frequency with droplet size needs to be investigated in depth since the contrary trends were often obtained from different models of breakage frequency even in the same conditions.

Therefore, it will be valuable to develop a novel or improved breakage model of droplet to consider the above aspects. Based on our previous work[26] that considered the main binary, ternary and quaternary breakages in the framework of inertia subrange, this work aims to develop such an improved multiple breakages model in the framework of wide energy spectrum. The contribution of the previous interactions between the droplet and the surrounding fluid to the breakage will be considered through introducing the interaction forces.

Model Development

The droplet breakage processes are usually very complex in turbulent dispersions. Therefore, some assumptions and representations are needed.

1. The breakage is mainly caused by turbulence.

In general, more than one breakage mechanism may exist in turbulent dispersions, since a droplet is not only exposed to a turbulent field but also subjected to internal viscous force. However, we focus on the breakage of low viscous droplet, and the viscous force could be neglected since the Ohnesorge number is usually quite small.

2. The possible nonexchangeability among the sizes of daughter droplets should depend on the processes of forming them in a given breakage.

Hill and Ng[27] argued that the integral of joint probability function did not depend on the forming processes of daughter solid particles as a whole, and treated all the volumes of the daughter solid particles as exchangeable. It seems equivalent to that all the daughter solid particles can be viewed as simultaneously formed by the same process. Diemer and Olson[28] argued that whether this treatment is suitable for droplets depends on the breakage process since the breakage of solid particle is essentially different from that of droplet. The experiments[21,23–25] have shown that the shape of droplet surface varies with time. Although the accurate time of forming each daughter droplet cannot be known from these experiments, we might as well think that all the daughter droplets are unlikely formed precisely at the same time in the case of ternary and quaternary breakages. That is, the daughter droplets are order-formed, and the constraints for the processes of forming each daughter droplet in a given multiple breakage may be different.

3. Both small eddies (equal to and smaller than the size of droplets) and large eddies (larger than the size of droplets) contribute to breakage.

Although most of the existing models assumed that only small eddies can cause breakage, the experiments showed that the large scale deformations often occurred.[21,24,29] Thus, the contribution of large eddies to breakage may also need to be considered. Based on inertial subrange spectrum, a mechanism for the breakage caused by large eddies was proposed by Han et al.,[26,30] this mechanism will be extended to multiple breakages (i.e., the main binary, ternary, and quaternary breakages) in the wide energy spectrum range.

4. The breakage frequency density and DSD can be represented as the functions about a general daughter-size fraction f_v or f_d.

The DSD in terms of a general size fraction f_v is usually needed for PBE. Nevertheless, the breakages represented by this general variable will include several different types of breakages when parent droplet breaks into more than two daughter droplets. This is because more than one size fraction exists (i.e., $f_{v,1}$, $f_{v,2}$, etc.) and then at least one of these size fractions equals to f_v. Later on, we will consider the possible breakage types with the general variable in detail.

Several turbulence parameters

To consider the multiple breakage process in the range of wide energy spectrum, we need to estimate the mean turbulent velocity $\bar{u}_k$, the mean turbulent kinetic energy $\bar{e}(k)$ and the number density of eddies n_k first. According to Lamont and Scott,[31] there is a proportional relationship among the amplitude of turbulent velocity A, the wave number k and the energy spectrum $E(k)$, namely, $A \approx \sqrt{kE(k)}$. Furthermore, according to Luk and Lee,[32] $\bar{u}_k \propto A$. Therefore

$$\bar{u}_k \propto \sqrt{kE(k)} = C_0\sqrt{kE(k)} \tag{1}$$

This relationship seems acceptable since the larger $E(k)$ usually indicates the higher turbulent kinetic energy contained in the eddies of given k, and $\bar{u}_k$ is thus higher. Based on the isotropic turbulent theory, the energy spectrum in the inertial subrange can usually be approximately expressed as $C\varepsilon^{2/3}k^{-5/3}$, where C is the Kolmogorov constant. Substituting this expression to Eq. 1, we could obtain $\bar{u}_k \propto \varepsilon^{1/3}k^{-1/3} \propto \varepsilon^{1/3}\lambda^{1/3}$. It is consistent with that obtained from second-order velocity structure functions.[33,34] Notice that the universal $\bar{u}_k$ in the energy containing range is still difficult to be obtained at present as the accurate turbulent structure for this range is not fully clear.[33] In this work, the characteristic mean turbulent velocity in inertia subrange is used to estimate the coefficient C_0. Thus, C_0 is estimated as $\sqrt{2}(2\pi)^{1/3}/\sqrt{C}$.

If the turbulent fluids could be viewed as a series of turbulent eddies with certain volume, the mean turbulent kinetic energy of eddies of wave number k could be represented by $(\rho_c u_k^2/2)\pi\lambda^3/6$. Substituting Eq. 1 and $\lambda = 2\pi/k$ into this formula, we can obtain

$$\bar{e}(k) = \frac{2}{3}\pi^4 C_0^2 \rho_c \frac{E(k)}{k^2} \tag{2}$$

The turbulent kinetic energy per unit mass contained in eddies of wave number between k and $k+dk$ can be expressed as

$$\hat{e}_{k\sim k+dk} = \rho_c(1-\alpha_d)\int_k^{k+dk} E(k)dk \tag{3}$$

where α_d is the volume fraction of dispersed phase. If dk is a very small value (e.g., it trends to zero), Eq. 3 can be expressed as

$$\hat{e}_{k\sim k+dk} \approx \rho_c(1-\alpha_d)E(k)dk \tag{4}$$

In addition, the turbulent kinetic energy per unit mass contained in eddies of wave number between k and $k+dk$ could also be obtained from $[(\rho_c u_k^2/2)\pi(2\pi/k)^3/6]n_k dk$. Thus, we can obtain

$$n_k \rho_c \frac{\pi}{6}\left(\frac{2\pi}{k}\right)^3 \frac{\bar{u}_k^2}{2}dk = \rho_c(1-\alpha_d)E(k)dk \tag{5}$$

Notice that $n_k dk$ could approximately denote the number of turbulent eddies of wave number between k and $k+dk$ when dk is a very small value.

Substituting Eq. 1 into Eq. 5, the number density of turbulent eddies of wave number k can be obtained as

$$n_k = \frac{3(1-\alpha_d)}{2\pi^4 C_0^2}k^2 \tag{6}$$

As seen from 1 and 2, the energy spectrum function $E(k)$ needs to be given first before the turbulence parameters can be used to establish the breakage model. To our knowledge, only two wide energy spectrum models that contain the dissipation range, the inertia subrange and the energy containing range can be found in the literature. The first is proposed by Pope.[33] According to Hinze,[35] the second energy spectrum model could be obtained through combining the energy spectrum from Kolmogorove scale to inertia subrange[36] and the energy spectrum from inertia subrange to energy containing range.[37]

The energy spectrum function proposed by Pope[33] can be written as

$$E(k) = C\varepsilon^{2/3}k^{-5/3}\left\{\frac{k\lambda_e}{\left[(k\lambda_e)^2+C_L\right]^{1/2}}\right\}^{5/3+P_0} \exp\left\{-\beta_2\left[(k\eta)^4+C_\eta^4\right]^{1/4}+\beta_2 C_\eta\right\} \tag{7}$$

where, P_0=2, β_2=5.2, $C_L \approx 6.78, C_\eta \approx 0.40$. Equation 7 can also written as $E(k)=C\varepsilon^{2/3}k^{-5/3}f_L f_\eta$. Where, f_L and f_η are specified nondimensional functions. $f_L=\{k\lambda_e/[(k\lambda_e)^2+C_L]^{1/2}\}^{11/3}$, which determines the spectrum shape of the energy containing range, and tends to unity for large $k\lambda_e$; $f_\eta = \exp\{-\beta_2[(k\eta)^4+C_\eta^4]^{1/4}+\beta_2 C_\eta\}$, which determines the spectrum shape of the dissipation range and tends to unity for small $k\eta$. In the inertia subrange, both f_L and f_η are essentially unity, so the Kolmogorov $-5/3$ spectrum with constant C is recovered. Notice that the original value of the Kolmogorov constant C given by Pope[33] is 1.5, but it is adjusted as 1.62 based on the direct numerical simulation (DNS)[38,39] and the experimental results of Sreenivasan.[40]

According to Hinze,[35] the energy spectrum from Kolmogorove scale to inertia subrange[36] can be written as

$$E(k) = (\varepsilon\nu^5)^{1/4}\left[1.61(k\eta)^{-5/3}+2.5(k\eta)^{-1}\right]\exp\left[-2.41(k\eta)^{4/3}-2.5(k\eta)^2\right] \tag{8}$$

And the energy spectrum from inertia subrange to energy-containing range can be defined through Von-Karman function[37]

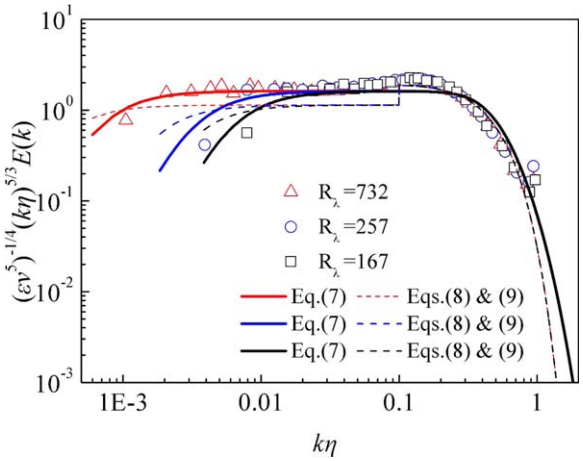

Figure 1. Comparison of the results predicted by different energy spectrum models with the results of DNS.

[Color figure can be viewed in the online issue, which is available at wileyonlinelibrary.com.]

$$E(k) = \frac{1.703u'2\lambda_e(k\lambda_e)^4}{\left[1+(k\lambda_e)^2\right]^{17/6}} \tag{9}$$

The energy spectrum distributions predicted by the Pope's spectrum with C=1.62 (i.e., Eq. 7) and the second spectrum (i.e., Eqs. 8 and 9) were shown in Figure 1. It can be seen that the results predicted by the Pope's spectrum show a better agreement with the DNS results.[39] Therefore, the Pope's spectrum with C=1.62 will be adopted to calculate the turbulence parameters.

In addition, the mean size of containing-energy eddy λ_e appearing in Eq. 7 should be determined first before the wide energy spectrum can be used. The main method of estimating λ_e is to measure Taylor microscale[41] or device characteristic size.[42,43] According to the relationship between ε and $E(k)$, however, Han et al.[44] proposed an expression to theoretically estimate λ_e, that is, $\varepsilon = 2\nu\int_{k_{min}}^{k_{max}} k^2 E(k)dk$. When $\theta_{min} \le 0.01$ ($\theta_{min}=2\pi\eta/\lambda_{max}$, λ_{max} could be taken as the diameter of impeller or bubble column D_{im}), $\lambda_e \approx 82.43\eta$. This approximate relationship will also be used since the condition of $\theta_{min} \le 0.01$ (e.g., $D_{im}>0.03$m, $\varepsilon>0.25$ m^2 s^{-3} and $\nu<1.1\times10^{-6}$ m^2 s^{-1}) can be easily satisfied in low viscous liquid–liquid systems mentioned later.

Notice that the recent work of Ghasempour et al.[45] presented a new function of number density of eddies, that is, $n_\lambda \propto \lambda^{-4} f_L f_\eta$ (or $n_k \propto k^2 f_L f_\eta$) from the energy conservation (i.e., Eq. 5) and the energy spectrum function proposed by Pope.[33] They extended the mean turbulent velocity of eddies $\bar{u}_\lambda \approx \alpha_0(\varepsilon\lambda)^{1/3}$ to the entire energy spectrum (where α_0 is a constant independent of λ). But this velocity distribution may mean that the ratio of $\bar{u}_\lambda$ to $(\varepsilon\lambda)^{1/3}$ will be a constant approximately in the entire size range of eddies. It seems different from that predicted by DNS.[34] When η is given, the normalized second-order structure function (i.e., $u_\lambda^2/(\varepsilon\lambda)^{2/3}$) predicted by DNS showed an obvious increase with increasing eddy size in the dissipation range, while this normalized structure function showed an obvious decrease with increasing eddy size in the energy containing range. Thus, the number density function proposed by Ghasempour et al.[45] may need to be further tested although the large eddy simulation

performed by them seems to support it. The ratio of $\bar{u}_\lambda$ to $(\varepsilon\lambda)^{1/3}$ estimated by Eq. 1 can give the consistent evolution trend with the DNS results. But as mentioned before, the universal $\bar{u}_k$ in the energy containing range is still difficult to be obtained at present. In this work, Eqs. 1 and 6 are adopted to establish the breakage model.

Surface deformation and oscillation

The high-speed camera was used by many investigators to observe the breakage processes of droplets or bubbles.[10,21,23–25,29] According to those typical pictures of droplets or bubbles breakage, droplets or bubbles may not be spherical after entering the flow field due to the possible surface deformation and oscillation.

Eastwood et al.[24] found that the surface oscillation takes place when the droplet begins to interact with the surrounding fluid. Nevertheless, the droplet does not break up at once. After a succession of such interactions, the droplet is fully deformed and the breakage occurs finally. The surface oscillation of bubbles was observed by Risso and Fabre[29] in a turbulent flow field through high-speed camera. They concluded that the oscillated bubble might accumulate the energy of deformation when it interacted with those eddies having no enough energy to cause immediate breakage.

As seen from these experimental observations, the contribution of surface oscillation to breakage needs to be considered. However, most of the existing models neglected the surface oscillation resulting from the previous collision or interaction between a fluid particle and an eddy. That is, the initial shape of parent fluid particle was usually assumed to be spherical. Han et al.[30] considered the effect of surface oscillation on the collision frequency between a droplet and an eddy through introducing a larger collision tube. Nevertheless, they assumed that the oscillation approximately obeys a sinusoidal function (i.e., $X=A_x\sin(2\pi t/T)$, X is the oscillating distance of surface). This assumption seems too simple and cannot directly reflect the interaction between the droplet and the surrounding fluid. In addition, the effect of the oscillation on the breakage probability (or breakage constraint) was not considered in their work.[30]

Based on the interaction forces between the droplet and the surrounding fluid, the effects of surface tension force, viscous force and turbulent fluctuation pressure on the surface deformation of droplets were investigated by Clark.[46] Clark[46] proposed that the variation of the position of mass center of the half droplet could be viewed as a vibration system analogous to the translation mechanical system. That is, the droplet could be viewed as two parts with half volume, and then the two parts are linked by a spring. Based on this mode, the equation of the dimensionless instantaneous distance (i.e., $y(t)$) of the mass centre of half oscillated droplet from its original position could be obtained as

$$\alpha_1\frac{d^2y(t)}{dt^2}+\alpha_2\frac{dy(t)}{dt}+\alpha_3 y(t)-F_{\mathrm{p}}=0 \tag{10}$$

where $y(t)=y'(t)/r_0$, $y'(t)$ denotes the deviation of mass center from y_0, and y_0 is the original position of mass center. In Eq. 10, $\alpha_1=0.5\pi r_0^3\rho_d$, $\alpha_2=9\pi^3\mu_{\mathrm{d}}r_0/8$, $\alpha_3=9\pi^3\sigma/8$, F_{p} denotes the turbulent fluctuation pressure. The first three terms on the left hand of Eq. 10, from left to right, denote the inertia force, viscous force, and surface tension force. In this work, the viscous force could be neglected since the low viscosity systems are studied. F_{p} could be written as $r_0\rho_c u_s^2$ according to Clark.[46]

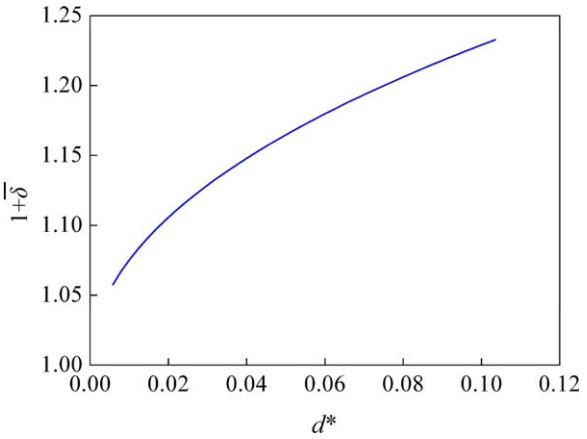

Figure 2. The mean surface oscillation degree given by Eq. 13 vs. d^*. ($d^*=d_0/L_{\mathrm{p}}$, $L_{\mathrm{p}}=(\sigma/\rho_{\mathrm{c}})^{3/5}\varepsilon^{-2/5}$).

[Color figure can be viewed in the online issue, which is available at wileyonlinelibrary.com.]

In this work, we assume that the distance (i.e., $y'(t)$) can roughly denote the distance of oscillated surface from its original position. That is, $y(t)\approx\delta/r_0$. Where, r_0 is the radius of undeformed droplet, δ is the surface oscillation distance. Combining Eq. 10 and the initial condition of $y(t)=0$ at $t=0$, we can obtain the solution to Eq. 10 as

$$y(t)=\alpha_4\sin\left(\frac{2\pi}{T}t\right)+\frac{8r_0\rho_{\mathrm{c}}\bar{u}_{\mathrm{s}}^2}{9\pi^3\sigma}\left[1-\cos\left(\frac{2\pi}{T}t\right)\right] \tag{11}$$

where, T is the period of surface oscillation $(=(4/3)\sqrt{\rho_{\mathrm{d}}r_0^3/\sigma})$, α_4 is a constant, and $\bar{u}_{\mathrm{s}}$ denotes the mean characteristic velocity of surface oscillation. Following Han et al.,[30] the mean oscillation velocity is assumed to equal to the mean fluctuation velocity of the surrounding fluid. That is, $\bar{u}_{\mathrm{s}}\approx\bar{u}(d_0)$. This assumption seems acceptable since the clean surface of droplet may be fully driven by turbulent fluctuations of the surrounding fluid. Here, $\bar{u}(d_0)$ can be obtained from Eq. 1, and $\bar{u}_{\mathrm{s}}$ could be estimated from the following expression

$$\bar{u}_{\mathrm{s}}\approx\frac{4}{T}\int_0^{T/4}\left[\frac{dy'(t)}{dt}\right]dt \tag{12}$$

Therefore, the mean surface oscillation distance of droplets can be written as

$$\bar{\delta}=\frac{\bar{u}_{\mathrm{s}}T}{2\pi}+\left(1-\frac{4}{\pi}\right)\frac{8r_0^2\rho_{\mathrm{c}}\bar{u}_{\mathrm{s}}^2}{9\pi^3\sigma} \tag{13}$$

As shown in Figure 2, $(1+\bar{\delta}/r_0)$ predicted by Eq. 13 is about 1.05–1.25 when d_0=0.5–2.5 mm, ε=3.7–16.4 $\mathrm{m^2\ s^{-3}}$, σ=0.053 $\mathrm{N\ m^{-1}}$, ρ_{c}=1000 $\mathrm{kg\ m^{-3}}$ and ρ_{d}=750 $\mathrm{kg\ m^{-3}}$, while the experimental data of Andersson and Andersson[21] is about 1.1–1.3. It indicates that the predicted results are in reasonable agreement with the experimental data. Notice that the specific range of d_0 was not given in the experiment, but the size of droplets was comparable to or close to 1.0 mm according to the other paper of Andersson and Andersson.[47]

To consider the effect of surface oscillation resulting from previous interactions between droplet and eddy on breakage, we imagine that the mean shape of parent droplet caused by this oscillation may become ellipsoidal. Such an ellipsoidal

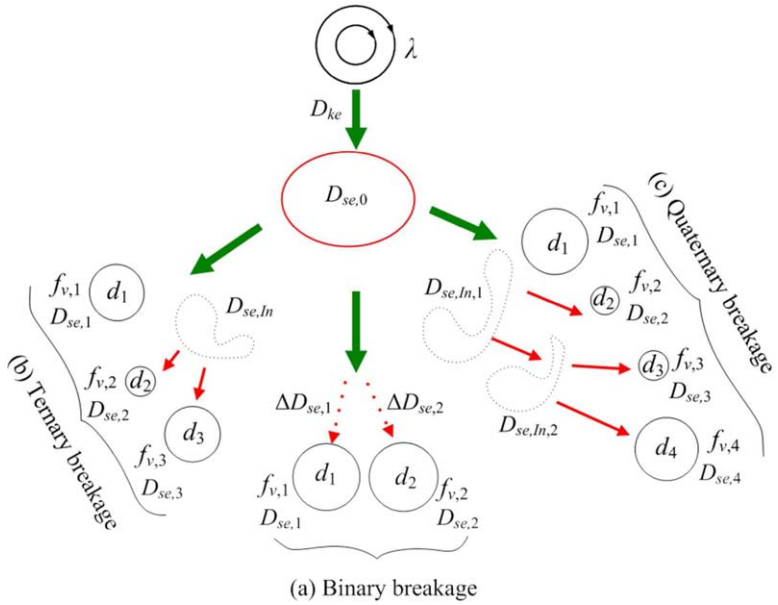

Figure 3. Sketch of binary, ternary and quaternary breakages.

[Color figure can be viewed in the online issue, which is available at wileyonlinelibrary.com.]

droplet has a long semiaxis (i.e., b) and two short semiaxses (i.e., a). Therefore, the surface area of the ellipsoidal droplet can be expressed as

$$S = 2\pi a^2\left\{1+\frac{\zeta}{2\sqrt{\zeta-1}}\times\left[\frac{\pi}{2}+\arcsin\left(\frac{\zeta-2}{\zeta}\right)\right]\right\} \tag{14}$$

where, $\zeta=b^2/a^2$, $b=r_0+\bar{\delta}$. According to the volume conservation (i.e., $4\pi r_0^3/3 = 4\pi a^2 b/3$), a can be obtained as $r_0(1+\bar{\delta}/r_0)^{-1/2}$. Equation 14 will be used to establish the breakage model through considering the effect of the mean shape of parent droplet on the breakage constraints and the collision or interaction frequency latter. In addition, the volume of parent droplet will be denoted by $\pi d_0^3/6$ in the following text, d_0 denotes the equivalent diameter of droplet.

Constraints of multiple breakages

Based on the framework of inertia subrange and the assumption of binary breakage, the constraint of surface energy density increase has been proposed by Han et al.[30] In this work, we will extend this constraint to multiple breakages in the framework of wide energy spectrum range.

As shown in Figure 3a, the surface energy density $D_{se,i}$ of daughter droplet i (i.e., surface energy per unit volume, $D_{se,i} = \pi d_i^2\sigma/\left(\pi d_i^3/6\right) = 6\sigma/d_i$) will increase in comparison with that of its equivalent volume in the parent droplet (i.e., $D_{se,0} = S\sigma/\left(\pi d_0^3/6\right)$, S is the surface area of parent droplet), since the volume of parent droplet is divided into several fragments while the total volume is not changed after breakage. Therefore, it may be expected that the energy density of parent droplet obtained from turbulent eddy should be equal to or more than the maximum of surface energy density increases of all daughter droplets. That is

$$D_{\mathrm{ke}} \geq \max\left(\Delta D_{\mathrm{se},1}, \Delta D_{\mathrm{se},2}\right) = \max\left(D_{\mathrm{se},1}, D_{\mathrm{se},2}\right) - D_{\mathrm{se},0} \tag{15}$$

where D_{ke} denotes the energy density of parent droplet, $D_{ke} = e(d_0)/\left(\pi d_i^3/6\right)$, $e(d_0)$ is the kinetic energy obtained from turbulent eddy of parent droplet, d_i is the diameter of daughter droplet i, $\Delta D_{\mathrm{se,i}}=D_{\mathrm{se,i}}-D_{\mathrm{se},0}$ (i=1, 2). Notice that, most of the existing models assumed that the shape of daughter droplets is spherical. This assumption is also adopted in this work, but the full deformation of the intermediates will be considered in the case of ternary and quaternary breakages (please see Figures 3b,c). Furthermore, the proposed constraint (i.e., Eq. 15) does not need to sum all $D_{\mathrm{se,i}}$ like to the constraint of surface energy increase, since it is based on the energy increase per unit volume. That is, if D_{ke} is equal to or more than the maximum of the density increases, other $\Delta D_{\mathrm{se},i}$ will also be satisfied.

In the literature, it was usually assumed that the kinetic energy of turbulent eddy could be fully utilized by the droplet with clean surface, namely, $e(k)\approx e(d_0)$. Equation 15 can be transformed into the following energy constraint

$$e(k) \geq \pi d_0^2\sigma\left\{\max\left[{f_{\mathrm{v},1}}^{-1/3}, \left(1-f_{\mathrm{v},1}\right)^{-1/3}\right]-S_{\mathrm{d}}\right\} \tag{16}$$

where S_{d} is a shape factor $\left(=S/\left(\pi d_0^2\sigma\right)\right)$, $f_{\mathrm{v},1}=(d_1/d_0)^3$, d_1 is the diameter of daughter droplet 1 shown in Figure 3a, and S can be determined from Eq. 14.

According to the experimental studies,[10,21,25] we propose that the ternary breakage of droplet could be composed of the following subprocesses (please see Figure 3b). That is, the parent droplet experiences a fully deformation and elongation first, then one part of the deformed and elongated body is split and becomes daughter droplet of size d_1 (i.e., the first subprocess), and the residual part of this body (which is also called intermediate in this work) subsequently breaks into two daughter droplets of sizes d_2 and d_3 (i.e., the second subprocess). Applying the constraint of surface energy density increase to ternary breakage, we can obtain

$$D_{\mathrm{ke}} \geq \left[\max\left(D_{\mathrm{se},1}, D_{\mathrm{se,In}}\right)-D_{\mathrm{se},0}\right]+\left[\max\left(D_{\mathrm{se},2}, D_{\mathrm{se},3}\right)-D_{\mathrm{se,In}}\right] \tag{17}$$

where $D_{\mathrm{se,In}}$ denotes the surface energy density of intermediate (its volume is denoted by $\pi d_{\mathrm{In}}^3/6$, d_{In} is the equivalent diameter of intermediate), the first and second terms on the right-hand side of Eq. 17 denote the maximal surface energy density increases of the first and second subprocesses,

respectively. Notice that the maximal surface energy density increase of one breakage subprocess mainly contributes to the critical energy required for the current subprocess. As shown in Figure 3b, the ternary breakage is composed of the two subprocesses. Thus, the critical energy required for ternary breakage can be determined from the sum of the critical energies of the two subprocesses, namely, the sum of the maximal surface energy density increases of the two subprocesses.

It should be noted that the second subprocess shown in Figure 3b is different from the binary breakage process shown in Figure 3a, although two daughter droplets are also formed in the second subprocess. This is because the intermediate (which is the original droplet in the second subprocess) has been fully deformed, and thus it may be quite easy to break up. In other word, the critical energy required for the second subprocess may be much smaller than that required for the binary breakage shown in Figure 3a, when the volume of parent droplet and the volume of the intermediate are equal and the size fractions resulting from the two different breakages are also equal.

Equation 17 can be transformed into the following energy constraint

$$e(k) \geq \pi d_0^2 \sigma \{\{\max[{f_{\mathrm{v},1}}^{-1/3}, (1-f_{\mathrm{v},1})^{-1/3}] - S_{\mathrm{d}}\} + C_t\{\max[{f_{\mathrm{v},2}}^{-1/3}, (1-f_{\mathrm{v},1}-f_{\mathrm{v},2})^{-1/3}] - (1-f_{\mathrm{v},1})^{-1/3}\}\} \quad (18)$$

where, $S_d = S/\left(\pi d_0^2 \sigma\right)$, $f_{\mathrm{v},1}=(d_1/d_0)^3$, $f_{\mathrm{v},2}=(d_2/d_0)^3$.

According to the above discussion, the critical energy determined by the surface energy density increase may be markedly over-estimated if the full deformation of intermediate is not considered. Therefore, in Eq. 18, coefficient C_{t} is introduced to consider the effect of this deformation. C_{t} is placed in front of curly brace rather than $(1-f_{\mathrm{v},1})^{-1/3}$ to explicitly estimate the surface energy density increase required for breakage. Notice that we can also introduce two different unknown parameters to account for this effect on the first and second subprocesses, respectively. However, estimating an appropriate value of C_{t} can achieve this purpose actually. In addition, it also could reduce the number of unknown parameters. In general, C_{t} should be quite small (i.e., $C_{\mathrm{t}} \ll 1$) due to the full deformation of intermediate.

For quaternary breakage, we propose that the breakage could be divided into three subprocesses (please see Figure 3c). That is, after parent droplet becomes a complex body with full deformation and elongation, the droplet first breaks into a daughter droplet of size d_1 and an intermediate of size $d_{\mathrm{In},1}$ (i.e., the first subprocess), then the intermediate of size $d_{\mathrm{In},1}$ breaks into a daughter droplet of size d_2 and an intermediate $d_{\mathrm{In},2}$ (i.e., the second subprocess), the intermediate of size $d_{\mathrm{In},2}$ subsequently breaks into two daughter droplets of sizes d_3 and d_4 (i.e., the third subprocess). Notice that $d_{\mathrm{In},1}$ and $d_{\mathrm{In},2}$ are the equivalent diameters of intermediates. Applying the constraint of surface energy density increase to quaternary breakage, we can obtain

$$D_{\mathrm{ke}} \geq \left[\max\left(D_{\mathrm{se},1}, D_{\mathrm{se,In},1}\right) - D_{\mathrm{se},0}\right] + \left[\max\left(D_{\mathrm{se},2}, D_{\mathrm{se,In},2}\right) - D_{\mathrm{se,In},1}\right] + \left[\max\left(D_{\mathrm{se},3}, D_{\mathrm{se},4}\right) - D_{\mathrm{se,In},2}\right] \quad (19)$$

where the first, second, and third terms on the right hand side of Eq. 19 denote the maximal surface energy density increases of the first, second and third subprocesses, respectively. Although two daughter droplets are formed in the second and third subprocesses shown in Figure 3c, these two subprocesses are different from the binary breakage process shown in Figure 3a due to the full deformation of the intermediates. Therefore, coefficient C_{q} is introduced to account for the effect of the deformation. Eq. 19 can be transformed into the following energy constraint

$$e(k) \geq \pi d_0^2 \sigma \{\{\max[{f_{v,1}}^{-1/3}, (1-f_{v,1})^{-1/3}] - S_{\mathrm{d}}\} + C_{\mathrm{q}}[\max({f_{v,12}}^{-1/3}, {f_{v,2}}^{-1/3}) - (1-f_{v,1})^{-1/3} + \max({f_{v,3}}^{-1/3}, {f_{v,4}}^{-1/3}) - {f_{v,12}}^{-1/3}]\} \quad (20)$$

where, $S_d = S/\left(\pi d_0^2 \sigma\right)$, $f_{\mathrm{v},12}=1-f_{\mathrm{v},1}-f_{\mathrm{v},2}$, $f_{\mathrm{v},34}=f_{\mathrm{v},3}+f_{\mathrm{v},4}$, and $f_{\mathrm{v},4}=1-f_{\mathrm{v},1}-f_{\mathrm{v},2}-f_{\mathrm{v},3}$.

Applying the surface energy increase to the binary, ternary, and quaternary breakages, respectively, we can obtain the following general energy constraint

$$e(k) \geq \pi d_0^2 \sigma \left(\sum_{i=1}^{n} f_{\mathrm{v},i}^{2/3} - S_{\mathrm{d}}\right) \quad (21)$$

where, $f_{\mathrm{v},n}=1-\sum_{i=1}^{n-1} f_{\mathrm{v},i}$, $f_{\mathrm{v},i}=(d_i/d_0)^3$, $i=1,\ldots, n$. n=2, 3, 4 denote the binary, ternary, and quaternary breakages, respectively.

Combining the constraint of surface energy density increase and the constraint of surface energy increase, the final energy constraint for breakage can be written as

$$e(k) \geq \max(e_{\mathrm{D}}, e_{\mathrm{S}}) \quad (22)$$

where, e_{D} denotes the critical energy determined by Eq. 16 or Eq. 18 or Eq. 20, e_{S} denotes the critical energy determined by Eq. 21. Concretely, Eqs. 16 and 21 (where n=2) are used for binary breakage, Eqs. 18 and 21 (where n=3) are used for ternary breakage, and Eqs. 20 and 21 (where n=4) are used for quaternary breakage. In addition, the critical energy required for forming n daughter droplets $e_{\mathrm{critical},n}$ will be used to denote the term on the righthand of Eq. 22.e., $\max(e_{\mathrm{D}}, e_{\mathrm{S}})$) in the following text.

It should be pointed out that Eqs. 16, 18, and 20−22 are only suitable to the case of small eddies (i.e., $k \geq 2\pi/d_0$). In the next section, we will introduce the available energy $e_{\mathrm{available}}(k)$ to substitute $e(k)$ appearing in these above equations in the case of large eddies. This is because the large eddy could carry the droplet (i.e., the droplet could be transported in the eddy).[48] Therefore, only the partial kinetic energy of large eddy may be transferred to the droplet.

The available kinetic energy of large eddies

In this section, we will estimate the available kinetic energy for the breakage provided by large eddy through the turbulent velocity distribution in the eddy. An sinusoidal velocity distribution proposed by Luk and Lee[32] is adopted here (i.e., $u=A\sin(\pi r/\lambda)$). Here, r is the distance from the centroid of eddy, which ranges from 0 to $\lambda/2$, A is velocity magnitude in r direction ($\approx \pi \bar{u}_k/2$), and $\bar{u}_k$ is the mean turbulent velocity of eddy. This function describes a velocity decrease from maximum to zero in the eddy, which was also adopted by Han et al.[49] as an origin to derive a gas-liquid interface mass-transfer model based on wide spectrum eddy contact concept. The liquid-side mass-transfer coefficient predicted by this model showed a good

agreement with the reported experimental data under various turbulence levels.

The mean turbulent velocity at a separate distance of d_0 in an eddy could be roughly estimated by $\bar{u}=\int_0^{d_0/2} u dr/(d_0/2)$. Here, d_0 is used to denote the equivalent distance when the parent droplet is transported in the eddy. We assume that the droplet surface is subjected to the turbulent fluctuation with the mean velocity $\bar{u}$ when the droplet is transported in the eddy, and $e_{available}(k)/e(k) \approx u^2/u_k^2$. Combining this approximate relationship, the above integral for obtaining $\bar{u}$ and the velocity distribution $u=A\sin(\pi r/\lambda)$, we can obtain the available kinetic energy of eddy

$$e_{\text{available}}(k) \approx 4\left(\frac{2\pi}{kd_0}\right)^2 \sin^4\left(\frac{kd_0}{8}\right) e(k) \tag{23}$$

This estimation method seems reasonable since the available kinetic energy will be smaller than the total kinetic energy contained in the large eddy. That is, $e_{\text{available}}(k)<e(k)$ when $k<2\pi/d_0$ (i.e., $\lambda>d_0$).

Breakage probability, collision, and interaction frequency densities

Following the study on the breakage of fluid particle performed by Luo and Svendsen,[14] when a droplet of semiaxses a and b interacts with an arriving eddy of wave number k, the probability for the droplet to break into n daughter droplets is assumed to equal to the probability of the arriving eddy having a kinetic energy greater more than or equal to the critical energy required for the droplet breakage. This gives

$$P(k,a,b) = 1-\int_0^{\vartheta_{c,n}} \exp(-\vartheta)d\vartheta = \exp\left(-\vartheta_{c,n}\right) \tag{24}$$

where $\vartheta(=e(k)/\bar{e}(k))$ is the dimensionless energy, $\vartheta c_{,n}(=e_{\text{critical},n}/\bar{e}(k))$ is the critical dimensionless energy required for the breakage of forming n daughter droplets, and $e_{\text{critical},n}$ can be obtained from Eqs. 22 and 23.

In the case of small eddies ($k\geq 2\pi/d_0$), the collision frequency density between an unoscillated fluid particle and an eddy was proposed by Luo and Svendsen.[14] In this work, this frequency density is modified to account for the contribution of surface oscillation of parent droplet to the breakage. As shown in Figure 4, the collision tube formed by an ellipsoidal droplet and an eddy has an elliptical cross section (its area is approximately taken as $\pi a'b'$). Notice that the circular collision cross section is also likely, but its area (i.e., $\pi a'^2$) seems smaller than $\pi a'b'$. Thus, $\pi a'b'$ is adopted to calculate the maximal area of collision cross section in this work. Here, $a'=a+\lambda/2$, $b'=b+\lambda/2$, and $\lambda=2\pi/k$.

The collision frequency density between an eddy of wave number k and a droplet of size d_0 (or semiaxses a and b) can be expressed as $S_{ab}\bar{u}_k n_k n_d$. Where n_k is the number density of eddies of sizes between k and $k+dk$, n_d is the number of droplets per unit space volume, and $S_{ab}\approx\pi a'b'$. Then, the collision frequency density in the range of wide energy spectrum could be obtained as

$$\varpi_{\text{collision}}(k,d_0) \approx \frac{3k^{5/2}(1-\alpha_d)n_d}{2\pi^3 C_0}\left(a+\frac{\pi}{k}\right)\left(b+\frac{\pi}{k}\right)\sqrt{E(k)} \tag{25}$$

where $E(k)$ could be the wide energy spectrum function (i.e., Eq. 7). Notice that ϖcollision(k, d_0) and $P(k, a, b)$ in Eq. 24 can also be expressed as ϖcollision(k, a, b) and $P(k, d_0)$, respectively, since both a and b are related to d_0 (i.e., $a=r_0(1+\bar{\delta}/r_0)^{-1/2}$, $b=r_0(1+\bar{\delta})$, $r_0=d_0/2$).

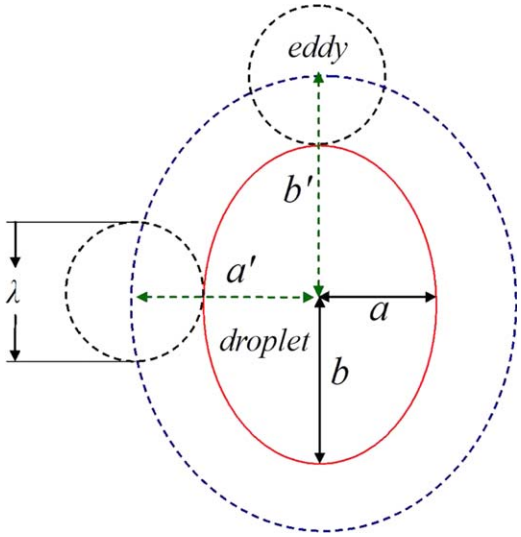

Figure 4. Sketch of collision cross section between turbulent eddy and deformed parent droplet.

[Color figure can be viewed in the online issue, which is available at wileyonlinelibrary.com.]

Nevertheless, Eq. 25 seems not suitable to the breakage caused by large eddies ($k<2\pi/d_0$) since the transport process of droplet in a large eddy cannot be reflected by such a collision. In general, this transport process may obviously reduce the chance of droplet contacting with the eddies. Thus, the interaction between a droplet and a large eddy may mainly be controlled by this process. Andersson and Andersson[47] proposed an interaction frequency density based on the concept of interaction volume per unit time which was calculated from the ratio of droplet volume to turnover time or lifetime of eddy. Han et al.[30] considered the effect of the transport time of droplet in an eddy since it is quite likely that the transport time is smaller than the lifetime of eddy. They estimated the interaction frequency density between a droplet and a large eddy as $V_0 n_k n_d/\min(\tau_e, \lambda/\bar{u})$. Here, V_0 is the equivalent volume of parent droplet determined by $\pi d_0^3/6$, τ_e is the lifetime of eddy (it approximately equals to $\lambda/\bar{u}_k$, $\bar{u}_k$ is determined by Eq. 1), n_k and $\bar{u}$ are determined by Eq. 6 and $\int_0^{d_0/2} u dr/(d_0/2)$, respectively. Notice that $\lambda/\bar{u}$ approximately denotes the transport time.

Then, the interaction frequency density in terms of general energy spectrum can be written as

$$\varpi_{\text{interaction}}(k,d_0) \approx \frac{(1-\alpha_d)k^{7/2}d_0^3 n_d}{8\pi^4 C_0} \max\left[1,\ \frac{4\pi}{kd_0}\sin^2\left(\frac{kd_0}{8}\right)\right]\sqrt{E(k)} \tag{26}$$

Breakage frequency densities of multiple breakages

The breakage frequency density of a droplet of size d_0 caused by an eddy of wave number k (which is also called partial breakage frequency density in this work) can be obtained from the product of the breakage probability and the collision or interaction frequency density. That is

$$\phi_n = \int_{k_{\min}}^{k_{\max}} \varpi(k, d_0) P(k, a, b) dk \tag{27}$$

where, n (=2, 3, 4) denotes the binary, ternary and quaternary breakages, respectively. $P(k, a, b)$ is calculated by Eq. 24. In the case of small eddies ($k \geq 2\pi/d_0$), ϖ (k, d_0)= ϖcollision(k, d_0)(i.e., Eq. 25). In the case of large eddies ($k<2\pi/d_0$), ϖ (k, d_0)= ϖinteraction(k, d_0) (i.e., Eq. 26).

For binary breakage, the partial breakage frequency density of droplet of volume V_0 breaks into two daughter droplets of sizes $f_v V_0$ and $(1-f_v)V_0$ can be written as

$$\varphi_2(f_v, V_0) = \phi_2 \tag{28}$$

where V_0 is the volume of droplet with semiaxses a and b (i.e., $\pi d_0^3/6$ or $4\pi a^2 b/3$), f_v is a general variable and denotes the size fraction(=$(d/d_0)^3$, d=d_1 or d_2 shown in Figure 3a).

Then, the overall breakage frequency density of droplet for binary breakage can be obtained as

$$\Omega_2(V_0) = \frac{1}{2}\int_0^1 \varphi_2(f_v, V_0) df_v \tag{29}$$

where the factor 1/2 takes into account that all the breakages will be counted twice when $\Omega_2(V_0)$ is calculated by integrating Eq. 29 over the range of $f_v \sim (0, 1)$. Notice that $\Omega_2(V_0)$ can also be expressed as $\Omega_2(a, b)$ since both a and b are related to d_0.

For ternary breakage, there are three daughter droplets of sizes $f_{v,1}V_0$ (or d_1), $f_{v,2}V_0$ (or d_2), and $f_{v,3}V_0$ (or d_3). The daughter droplets of size fractions $f_{v,1}$, $f_{v,2}$ (or $f_{v,3}$) seem statistically distinguishable or nonexchangeable one another, as the processes of forming them are different (please see Figure 3b). However, the daughter droplets of size fractions $f_{v,2}$ and $f_{v,3}$ are statistically indistinguishable or exchangeable each other since they are formed simultaneously from the same process. Thus, the breakages of forming three daughter droplets, which are denoted by a general size fraction f_v (=V/V_0), indicate three different types of breakages in which at least one of the volumes of three daughter droplets equals to V). Namely, $f_{v,1}$=f_v, $f_{v,2}$=f_v and $f_{v,1}$=$f_{v,2}$=f_v. Notice that the breakage type of $f_{v,1}$=f_v actually denotes that of $f_{v,1}$=f_v, $f_{v,2}\neq f_v$, and $f_{v,3}\neq f_v$, the breakage type of $f_{v,2}$=f_v actually denotes that of $f_{v,2}$=f_v, $f_{v,1}\neq f_v$, and $f_{v,3}\neq f_v$. For simplicity, the terms of $f_{v,i}\neq f_v$ (i=1, 2, 3) are not given in form. This method is also adopted to describe other types of breakages in this work, except for special statement. Nevertheless, the breakage type of $f_{v,1}$=$f_{v,2}$=f_v can include the equal-sized breakage event of $f_{v,1}$=$f_{v,2}$=$f_{v,3}$=f_v(=1/3). Here, $f_{v,3}$=$1-f_{v,1}-f_{v,2}$.

Then, the partial breakage frequency density for ternary breakage can be obtained as

$$\varphi_3(f_v, V_0) = \frac{1}{2}\int_0^{1-f_v} \phi_3 df_{v,2} + \int_0^{1-f_v} \phi_3 df_{v,1} \tag{30}$$

The first term on the right hand of Eq. 30 denotes the breakage type of $f_{v,1}$=f_v, and the second term denotes the breakage type of $f_{v,2}$=f_v. In the first term, when $f_{v,1}$(=f_v) is given, $f_{v,2}$ can vary in the range of (0, $1-f_{v,1}$). While the integrand ϕ_3 is symmetrical with $f_{v,2}$=$(1-f_{v,1})/2$ as the size fractions of $f_{v,2}$ and $f_{v,3}$ are statistically indistinguishable or exchangeable each other. For example, when $f_{v,1}$=0.3, $f_{v,2}$ can range from 0 to 0.7. The breakage denoted by $f_{v,1}$=0.3, $f_{v,2}$=0.5, and $f_{v,3}$=0.2 and the breakage denoted by $f_{v,1}$=0.3, $f_{v,2}$=0.2, and $f_{v,3}$=0.5 belong to the same breakage. Thus, the factor 1/2 appears in the first term. Conversely, when $f_{v,2}$(=f_v) is given and $f_{v,1}$ varies in the range of (0, $1-f_{v,2}$), the integrand ϕ_3 is unsymmetrical with $f_{v,1}$=$(1-f_{v,2})/2$ since the daughter droplets of sizes d_1 and d_3 are formed by different processes (correspondingly, the breakage constraints for forming the daughter droplets of sizes d_1 and d_3 are different from each other) and thus the size fractions of $f_{v,1}$ and $f_{v,3}$ are distinguishable or nonexchangeable. For example, when $f_{v,2}$=0.4, $f_{v,1}$ ranges from 0 to 0.6, the breakage denoted by $f_{v,2}$=0.4, $f_{v,1}$=0.1, and $f_{v,3}$=0.5 and the breakage denoted by $f_{v,2}$=0.4, $f_{v,1}$=0.5, and $f_{v,3}$=0.1 do not belong to the same breakage. Thus, the factor 1/2 does not appear in the second term. In addition, the breakage type of $f_{v,1}$=$f_{v,2}$=f_v can be included by the first term and the second term since $f_{v,2}$ can equal to f_v in the first term and $f_{v,1}$ also can equal to f_v in the second term. Thus, to avoid counting these types of breakages repeatedly, the condition of $f_{v,2}\neq f_v$ in the first term or $f_{v,1}\neq f_v$ in the second term needs to be satisfied.

The overall breakage frequency density for ternary breakage can be obtained as

$$\Omega_3(V_0) = \frac{1}{3}\int_0^1 \varphi_3(f_v, V_0) df_v \tag{31}$$

where the factor 1/3 takes into account that the breakages will be counted three times when $\Omega_3(V_0)$ is calculated by integrating Eq. 30 over the range of $f_v \sim (0, 1)$. For example, the breakage represented by f_v (i.e., $f_{v,1}$)=0.3 and $f_{v,\ 2}$=0.6 in the first term on the right hand of Eq. 30, and the breakage represented by f_v (i.e., $f_{v,2}$)=0.6 and $f_{v,1}$=0.3 in the second term on the right hand of Eq. 30 are the same breakage. Notice that when the second term on the right hand of Eq. 30 is integrated over the whole range of $f_v \sim (0, 1)$, the breakages represented by the second term will be counted twice. For example, the breakage represented by f_v (i.e., $f_{v,2}$)=0.6 and $f_{v,1}$=0.3, and the breakage represented by f_v (i.e., $f_{v,2}$)=0.1 and $f_{v,1}$=0.3 are the same breakage since $f_{v,2}$=0.6 (correspondingly, $f_{v,3}$=0.1) an $f_{v,2}$=0.1(correspondingly, $f_{v,3}$=0.6) actually correspond to the same breakage process (please see Figure 3b). Therefore, the total breakages will be counted three times in the range of $f_v \sim (0, 1)$.

It should be noted that the two integrals on the right hand of Eq. 30 are necessary for obtaining $\varphi_3(f_v,V_0)$. This is because the definition of $\varphi_3(f_v,V_0)$ is based on a given and general daughter droplet size fraction f_v, which is usually required for DSD in PBE. As mentioned before, the breakages that are denoted by a given size fraction f_v indicate that at least one of the size fractions of three daughter droplets equals to f_v. Thus, three different types of breakages mentioned above need to be included and contribute to $\varphi_3(f_v,V_0)$. Notice that the condition of $f_{v,2}\neq f_v$ in the first integral of Eq. 30 or $f_{v,1}\neq f_v$ in the second integral of Eq. 30 is not necessary for Eq. 31 when the overall breakage frequency density, $\Omega_3(V_0)$, is calculated.

For quaternary breakage, there are four daughter droplets of sizes $f_{v,1}V_0$ (or d_1), $f_{v,2}V_0$ (or d_2), $f_{v,3}V_0$ (or d_3), and $f_{v,4}V_0$ (or d_4). The size fractions of $f_{v,3}$ and $f_{v,4}$ are statistically indistinguishable or exchangeable each other since the daughter droplets of sizes d_3 and d_4 are formed simultaneously from the same process (please see Figure 3c). But, the size fractions of $f_{v,1}$, $f_{v,2}$, and $f_{v,3}$ seem statistically distinguishable or nonexchangeable one another since the processes of forming them are different. That is, the breakage

constraints for forming the daughter droplets of sizes d_1, d_2, and d_3 are different from one another. Thus, the breakages of forming four daughter droplets, which are denoted by a given size fraction f_v, indicate seven different types of breakages in which at least one of the size fractions of daughter droplets equals to f_v. Namely, $f_{v,1}=f_v$, $f_{v,2}=f_v$, $f_{v,3}=f_v$, $f_{v,1}=f_{v,2}=f_v$, $f_{v,1}=f_{v,3}=f_v$, $f_{v,2}=f_{v,3}=f_v$, and $f_{v,1}=f_{v,2}=f_{v,3}=f_v$. Notice that the breakage type of $f_{v,1}=f_{v,2}=f_{v,3}=f_v$ can include the equal-sized breakage event of $f_{v,1}=f_{v,2}=f_{v,3}=f_{v,4}=f_v$ (=1/4). Here, $f_{v,4}=1-f_{v,1}-f_{v,2}-f_{v,3}$.

Then, the partial breakage frequency density for quaternary breakage can be obtained as

$$\varphi_4(f_v,V_0)=\left(\sum_{j=1}^{2}\int_0^{1-f_v}\int_0^{1-f_v-f_{v,l}}\frac{\phi_4}{2}df_{v,h}df_{v,l}\right)+\int_0^{1-f_v}\int_0^{1-f_v-f_{v,1}}\phi_4 df_{v,2}df_{v,1} \tag{32}$$

where $h=(j+1)(4-j)/2$, $l=1+(j-2)(j-3)/2$, $j=1, 2$. The subscripts h and l obtained from Lagrange polynomial interpolation method are introduced to make Eq. 32 into a general form. The first term (j=1) on the right hand of Eq. 32 denotes the breakage type of $f_{v,1}=f_v$, the second term (j=2) denotes the breakage type of $f_{v,2}=f_v$, and the third term denotes the breakage type of $f_{v,3}=f_v$. Note that the breakage types of $f_{v,1}=f_{v,2}=f_v$, $f_{v,1}=f_{v,3}=f_v$, $f_{v,2}=f_{v,3}=f_v$, and $f_{v,1}=f_{v,2}=f_{v,3}=f_v$ can be included in Eq. 32. In addition, the conditions of $f_{v,1}\neq f_{v,2}\neq f_v$, $f_{v,1}\neq f_{v,3}\neq f_v$ in the first term, and $f_{v,2}\neq f_{v,3}\neq f_v$ in the second term need to be satisfied to avoid counting these types of breakages repeatedly.

In the first term (j=1), when $f_{v,1}(=f_v)$ is given, $f_{v,2}$ can vary in the range of $(0, 1-f_{v,1})$ and $f_{v,3}$ can vary in the range of $(0, 1-f_{v,1}-f_{v,2})$. Similarly, in the second term (j=2), when $f_{v,2}(=f_v)$ is given, $f_{v,1}$ varies in the range of $(0, 1-f_{v,2})$ and $f_{v,3}$ varies in the range of $(0, 1-f_{v,2}-f_{v,1})$. In these cases, the integrand ϕ_4 is symmetrical with $f_{v,3}=(1-f_{v,1}-f_{v,2})/2$ since the size fractions of $f_{v,3}$ and $f_{v,4}$ are exchangeable each other. Thus, the factor 1/2 appears in the above two terms. Nevertheless, this factor does not appear in the third term. This is because when $f_{v,3}(=f_v)$ is given, $f_{v,1}$ varies in the range of $(0, 1-f_{v,3})$ and $f_{v,2}$ varies in the range of $(0, 1-f_{v,3}-f_{v,1})$, the integrand ϕ_4 is unsymmetrical with $f_{v,2}=(1-f_{v,3}-f_{v,1})/2$. In this case, the daughter droplets of sizes d_1, d_2, and d_4 (or d_3) are formed by different processes (please see Figure 3c), and the size fractions of $f_{v,1}$, $f_{v,2}$, and $f_{v,4}$ (or $f_{v,3}$) are statistically nonexchangeable one another.

The overall breakage frequency density for quaternary breakage can be obtained as

$$\Omega_4(V_0)=\frac{1}{4}\int_0^1\varphi_4(f_v,V_0)df_v \tag{33}$$

where the factor 1/4 takes into account that the breakages will be counted four times when $\Omega_4(V_0)$ is calculated through integrating Eq. 32 over the range of $f_v\sim(0, 1)$. For example, the breakage represented by f_v (i.e., $f_{v,1}$)=0.2 and $f_{v,2}$=0.3 and $f_{v,3}$=0.4 in the first term (j=1) on the right hand of Eq. 32, and the breakage represented by f_v (i.e., $f_{v,2}$)=0.3 & $f_{v,1}$=0.2 & $f_{v,3}$=0.4 in the second term (j=2), and the breakage represented by f_v (i.e., $f_{v,3}$)=0.4 & $f_{v,1}$=0.2 & $f_{v,2}$=0.3 in the third term are the same breakage. Notice that the breakages will be counted twice when the third term on the right hand of Eq. 32 is integrated over the whole range of $f_v\sim(0, 1)$. For example, the breakage represented by f_v (i.e., $f_{v,3}$)=0.4 & $f_{v,1}$=0.2 & $f_{v,2}$=0.3, and the breakage represented by f_v (i.e., $f_{v,3}$)=0.1 & $f_{v,1}$=0.2 & $f_{v,2}$=0.3 are the same breakage since $f_{v,3}$=0.4 & $f_{v,4}$=0.1 and $f_{v,4}$=0.1 & $f_{v,3}$=0.4 correspond to the same breakage process (please see Figure 3c). Therefore, the overall breakages will be counted four times in the range of $f_v\sim(0, 1)$. It should be noted that the three terms on the right hand of Eq. 32 are necessary for obtaining $\varphi_4(f_v,V_0)$ due to the reason similar to ternary breakage. As mentioned before, seven different types of breakages mentioned above need to be included and contribute to $\varphi_4(f_v,V_0)$.

For the parallel-competing decomposition reactions, that is, $R\rightarrow 2C$, $R\rightarrow 3D$, and $R\rightarrow 4E$, the overall reaction rate of R can be represented by the sum of the rates of the three reactions. Analogously, the overall breakage frequency density of droplet for multiple breakages can be expressed as

$$\Omega(V_0)=\sum_{n=2}^{4}\Omega_n(V_0) \tag{34}$$

where n=2, 3, 4.

DSD of multiple breakages

As mentioned before, the DSD in terms of a given and general daughter-size fraction f_v is usually needed for PBE. Following the distribution function proposed by Luo and Svendsen,[14] the DSD probability density function for multiple breakages can be written as

$$\beta(f_v,V_0)=\frac{\psi(f_v,V_0)}{\int_0^1\psi(f_v,V_0)df_v} \tag{35}$$

where, $\psi(f_v,V_0)$ describes the breakages represented by a given size fraction f_v, which indicates that at least one of the size fractions of the daughter droplets equals to f_v. Thus, there will be eleven different types of breakages contributing to the probability density $\beta(f_v,V_0)$ according to the analysis mentioned before. Namely, one type for binary breakage ($f_v=f_{v,1}$), three different types for ternary breakage, and seven different types for quaternary breakage). In Eq. 35, $\psi(f_v,V_0)$ can be obtained from $\sum_{n=2}^{4}\varphi_n(f_v,V_0)$.

Results and Discussions

Estimation of deformation factors

In this work, deformation factors, C_t and C_q appearing in Eqs. 18 and 20, need to be determined first. It should be pointed out that the upper limit of C_t or C_q can be taken as one in theory. But it means that there is no deformation of intermediates, and then the second or the third subprocess will be equivalent to a new binary breakage of parent droplet shown in Figure 3a. In general, the values of them should be quite small due to the full deformation of intermediates. The shapes of intermediates seem very complex, and it is difficult to obtain the accurate values of them. But we could estimate them from experimental results. In this work, C_t and C_q will be estimated from the breakage frequency.

Andersson and Andersson[47] measured the breakage frequency of dodecane droplets (σ=0.053N m^{-1}, μ_d=1.5 mPa s, ρ_d=750 kg m^{-3}) in a fully developed turbulent flow. Their experimental results showed that multiple breakages of low viscous droplets often occur[19] (i.e., the main binary, ternary and quaternary breakages) when turbulent dissipation rate ε

equals to 8.5 m^2 s^{-3}. It is found to be appropriate that C_t and C_q are taken as about 0.039 and 0.11 for ternary and quaternary breakages, respectively, through comparing the predicted breakage frequencies by Eq. 34 (where k_{max} and k_{min} are taken as $2\pi/\eta$ and $2\pi/(10d_0)$, respectively) with the experimental data of Andersson and Andsersson.[47] Please see the section of "Comparison with the experimental data and other models: breakage frequency." These two values are close to the parameters proposed by Han et al.[26] It should be pointed out that the breakages of forming more than four daughter droplets were also observed in the experiment of Andersson and Andersson,[21] but these breakages have a nearly negligible contribution to the overall breakage frequency as their frequencies are quite small. In the following sections, we will compare the predicted breakage frequencies and DSDs with other available experimental data to test the ability of the proposed model (i.e., Eqs. 27–35) with the two values applied to other low viscous liquid–liquid systems.

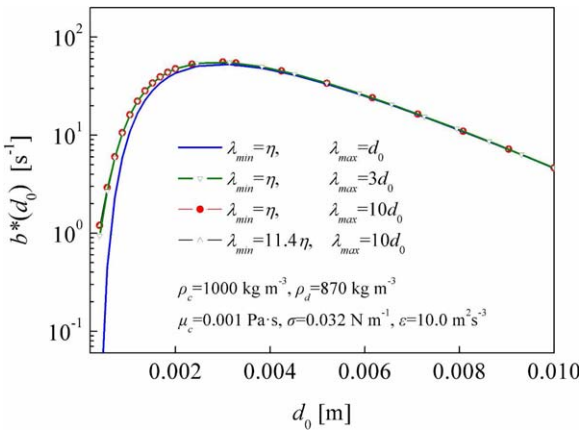

Figure 5. The effect of integral limits on specific breakage frequency.

[Color figure can be viewed in the online issue, which is available at wileyonlinelibrary.com.]

Effect of integral limits

The effect of integral limits, k_{min} (i.e., $2\pi/\lambda_{max}$) and k_{max} (i.e., $2\pi/\lambda_{min}$) appearing in Eq. 27, is tested in this section. Figure 5 shows the specific breakage frequency $b^*(d_0)$ $(=\Omega(V_0)/[(1-\alpha_d)n_d])$ predicted by Eq. 34. As seen from Figure 5, the eddies of size larger than $10d_0$ almost do not contribute to the overall breakage frequency. Thus, k_{min} could be taken as $2\pi/(10d_0)$. It is worth to be noted that the eddies of size equal to and smaller than $3d_0$ contribute to most of the overall breakage frequency. This trend could explain the experimental findings of Andersson and Andersson.[21] Their experiments showed that the droplets are subject to large scale deformations, that is, close in size to and up to three times larger than the droplet, prior to breakage, and the surface oscillation is obvious. It means that the contribution of the large eddies and the surface oscillation needs to be considered. The reason why large eddies do not contribute much to the overall breakage frequency is that the interaction frequency density between eddy and droplet is very low ($k^{7/2}$).

As shown in Figure 5, the eddies in the dissipation range (i.e., the eddies of size smaller than about 11.4η) nearly do not contribute to the overall breakage frequency in the condition of d_0=0.5–10 mm and ε=8.5 m^2 s^{-3}. This is because $E(k)$ in the dissipation range is much smaller than those in other ranges (notice that droplets are obviously larger in size than the eddies in this range at this time), which means that there are no enough kinetic energies for eddies to break the droplets. Therefore, the breakage frequency may be quite small in the dissipation range. However, it should be noted that the eddies of size smaller than 11.4η may also contribute to the overall breakage frequency in some operating conditions since the sizes of droplets may fall in the dissipation range. Thus, k_{max} appearing in Eq. 27 could be taken as $2\pi/\eta$.

Effect of energy spectrum

The effect of energy spectrum $E(k)$ on specific breakage frequencies of droplets has been shown in Figures 6a,b. The specific breakage frequency $b^*(d_0)$ of droplets can be predicted by the proposed model (i.e., Eqs. 27–34) coupled with the ESIS (i.e., $E(k)=C\varepsilon^{2/3}k^{-5/3}$). This spectrum is used to cover the energy containing range and the inertia subrange. The integral upper limit k_{max} in Eq. 27 is $2\pi/(11.4\eta)$ when the proposed model is coupled with ESIS. The results given by ESIS exhibit a monotonic increase with increasing d_0. While, $b^*(d_0)$ predicted by Eqs. 27–34 coupled with the wide energy spectrum function (i.e., Eq. 7) exhibits a nonmonotone behavior with increasing d_0. The similar nonmonotone trend has also been observed by experimental results of Maaβ and Kraume.[10] As shown in Figure 6a, the eddies of size larger than $3d_0$ or less than $0.1d_0$ nearly do not contribute to $b^*(d_0)$ of droplets in the condition given in Figure 6a. It may indicate that the breakage of droplets is mainly caused by the eddies of size comparable to or close to the size of droplets. In addition, the critical diameter d_c exhibits a decrease when ε increases. For example, d_c is about 2.8 and 2.3 mm when ε=10 and 20 m^2 s^{-3}, respectively.

As seen from Figure 6b, the ratio of the breakage frequencies predicted by Eq. 7 to the breakage frequencies predicted by ESIS, that is, Λ, shows a nonmonotone evolution with increasing parent droplet size d_0. In addition, our calculations show that the range of d_0 in which Λ is more than about 0.7 will not be obviously changed when the density of droplets and the surface tension are changed. Thus, the main factor that contributes to this range of d_0 is the turbulent dissipation rate ε in low viscous systems. According to Figure 6b, with the decreasing ε, the range of d_0 in which Λ is more than about 0.7 is also narrowed. For example, when ε=100 m^2 s^{-3}, d_0=0.08–1.0 mm; while when ε=50 m^2 s^{-3}, d_0=0.10–1.0 mm; when ε=20 m^2 s^{-3}, d_0=0.14–1.0 mm; when ε=5 m^2 s^{-3}, d_0=0.22–1.0 mm. The smaller ε means the narrower inertia subrange, and thus the difference between the breakage frequencies predicted by Eq. 7 and ESIS will be obvious gradually.

According to the difference between the wide energy spectrum (i.e., Eq. 7) and ESIS (please see Figure 6c), the nonmonotone behavior of breakage frequency will be explained in the following text through the relative relationship between the collision or interaction frequency density and the breakage probability. Based on Eqs. 7 and 25, the specific collision frequency density $\varpi^*_{collision}(k, d_0)$ (i.e., $\varpi collision(k, d_0)/[(1-\alpha_d)n_d]$) is proportional to $(a+\pi/k)(b+\pi/k)k^{5/3}(f_1 f_\eta)^{1/2}$ when ε is given, while for ESIS, $\varpi^*_{collision}(k, d_0)$ is proportional to $(a+\pi/k)(b+\pi/k)k^{5/3}$. Thus, for the eddies of size falling in the energy containing range, $\varpi^*_{collision}(k, d_0)$ predicted by Eq. 7 will be different from

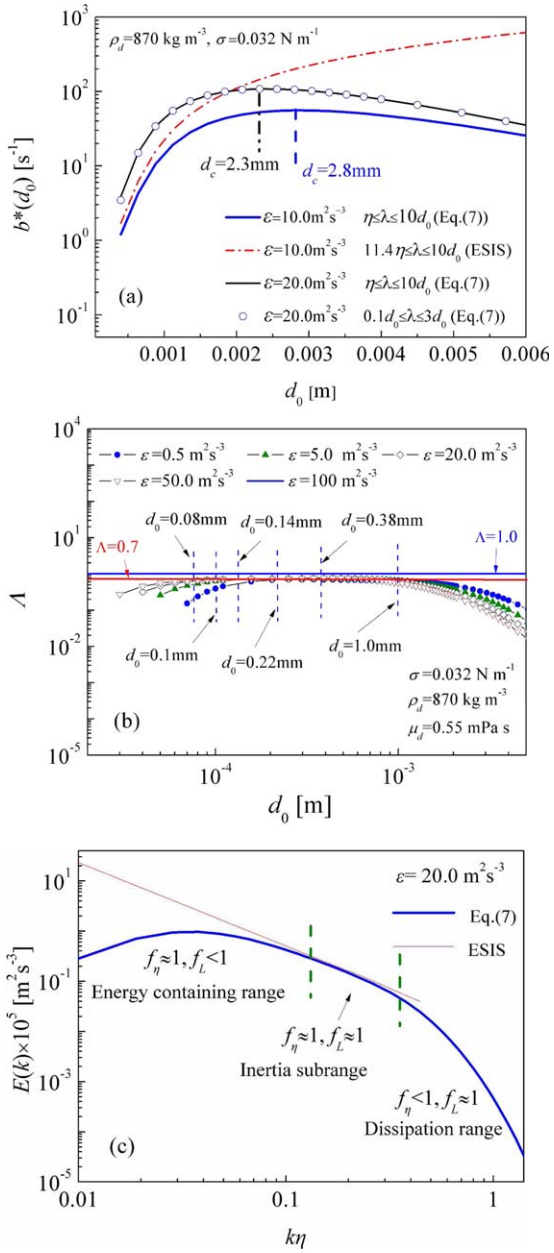

Figure 6. The effect of energy spectrum on specific breakage frequency. (μ_c=0.001Pa·s, ρ_c=1000 kg m^{-3}).

[Color figure can be viewed in the online issue, which is available at wileyonlinelibrary.com.]

that predicted by ESIS. That is, the former will be smaller than the latter since $f_L<1$ in the energy containing range. Figure 7a shows the examples for $\varpi^*_{collision}(k, d_0)$ in the energy containing range, the difference between the specific collision frequency densities predicted by Eq. 7 and ESIS seems to be larger when k decreases (or λ increases). Moreover, the predicted $\varpi^*_{collision}(k, d_0)$ increases with increasing d_0 when the size of eddy and ε are given. It should be noted that the evolution of the specific interaction frequency density of $\varpi^*_{interaction}(k, d_0)$ (i.e., ϖinteraction$(k, d_0)/[(1-\alpha_d)n_d]$) with increasing d_0 or decreasing k is similar to that of $\varpi^*_{collision}(k, d_0)$.

Conversely, as seen from Figure 7b, the breakage probability $P(k, d_0)$ decreases with increasing d_0 when the size of eddy and ε are given, but $P(k, d_0)$ increases with decreasing k (or increasing λ) when d_0 and ε are given. Thus, as a whole, the evolution of breakage frequency with increasing d_0 depends on the relative decrement of $P(k, d_0)$ and the relative increment of $\varpi^*_{collision}(k, d_0)$ or $\varpi^*_{interaction}(k, d_0)$. When the increment of $\varpi^*_{collision}(k, d_0)$ is smaller than the decrement of $P(k, d_0)$ when d_0 increases, $b^*(d_0)$ increases with d_0; while when the former is larger than the latter, $b^*(d_0)$ decreases with d_0. $b^*(d_0)$ exhibits a maximum when $d_0=d_c$ (i.e., the critical diameter). The nonmonotone evolution of $b^*(d_0)$ could attribute to the wide energy spectrum distribution. The distribution of the wide energy spectrum exhibits a nonmonotone behavior with decreasing k, which can be seen from $E(k)=C\varepsilon^{2/3}k^{-5/3}f_L f_\eta$. Here, both f_L and f_η are approximately equal to or smaller than unity, f_L decreases with decreasing k in the energy containing range and f_η decreases with increasing k in the dissipation range. This nonmonotone trend has an important influence on the relative decrement of $P(k, d_0)$ and the relative increment of $\varpi^*_{collision}(k, d_0)$ or $\varpi^*_{interaction}(k, d_0)$. For ESIS that exhibits a monotone increase with decreasing k (it can seen from $E(k)=C\varepsilon^{2/3}k^{-5/3}$), the increment of $\varpi^*_{collision}(k, d_0)$ or $\varpi^*_{interaction}(k, d_0)$ will be always larger than the decrement of $P(k, d_0)$, thus $b^*(d_0)$ predicted by ESIS monotonously increases with increasing d_0, please see Figure 7. Notice that only the binary breakage is discussed in Figure 7 since the similar trend for the ternary and quaternary breakages can also be obtained.

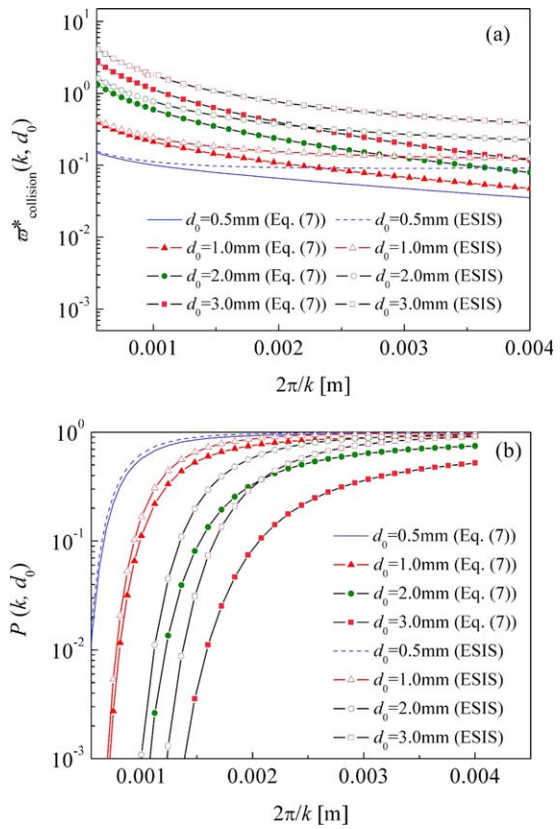

Figure 7. The effect of energy spectrum on collision frequency and breakage probability (f_v=0.2, ε=10 m^2 s^{-3}, μ_c=0.001 Pa s, ρ_c=1000 kg m^{-3}, ρ_d=870 kg m^{-3}, σ=0.032 N m^{-1}).

[Color figure can be viewed in the online issue, which is available at wileyonlinelibrary.com.]

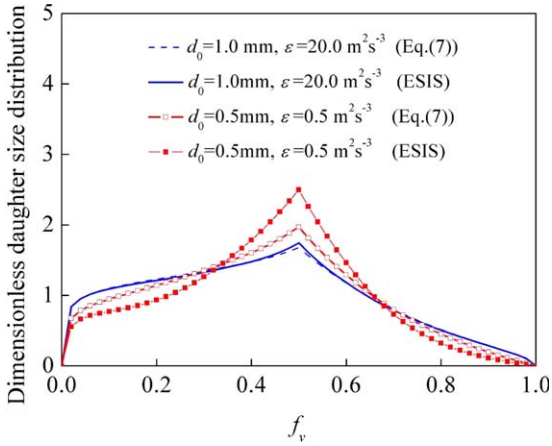

Figure 8. The effect of energy spectrum on DSD.(f_v=V/V_0, σ=0.002 N m^{-1}, ρ_c=1000 kg m^{-3}, ρ_d=760 kg m^{-3}, μ_c=0.001 Pa s).

[Color figure can be viewed in the online issue, which is available at wileyonlinelibrary.com.]

Based on the proposed model framework (i.e., Eqs. 27–35), the effect of energy spectrum on DSD is shown in Figure 8. As a whole, the DSD predicted by the proposed model coupled with Eq. 7 nearly coincides with that predicted by the proposed model coupled with ESIS in the condition of d_0=1.0 mm and ε=20 m^2 s^{-3}, while the DSD given by Eq. 7 exhibits a more flat distribution than that given by ESIS in the condition of d_0=0.5 mm and ε=0.5 m^2 s^{-3}. This is because that the sizes of droplets (i.e., 1.0 and 0.5 mm) fall in the inertia subrange and in the dissipation range, respectively, in the condition of ε=20 m^2 s^{-3} and ε=0.5 m^2 s^{-3}. According to Figure 6c, the difference between Eq. 7 and ESIS may be quite small near the inertia subrange and the eddies of size comparable to or close to d_0 may mainly contribute to breakage. Thus, the sizes of these eddies are also close to the inertia subrange and the difference between the DSDs predicted by Eq. 7 and ESIS will be quite small. When d_0=0.5 mm and ε=0.5 m^2 s^{-3}, as seen from Figure 8, the difference between the DSDs predicted by Eq. 7 and ESIS seems obvious since the fair amount of the eddies that mainly contribute to breakage will also fall in the dissipation range.

As seen from Figure 8, the predicted DSD profile of f_v<0.5 is obviously higher than that of f_v>0.5 due to the contribution of multiple breakage events. The DSD is symmetrical about f_v=0.5 for binary breakage process, while the DSD is asymmetrical both for the ternary and quaternary breakage processes, respectively. Namely, more small daughter droplets (f_v<0.5) will be formed through the ternary and quaternary breakage events. For example, there are two or three daughter droplets (f_v<0.5) are formed from a ternary breakage event, while there are three or four daughter droplets (f_v<0.5) are formed from a quaternary breakage event. Therefore, the higher profile of f_v<0.5 will appear for the multiple breakages. In the following text, the proposed model will be always coupled with the wide energy spectrum function (i.e., Eq. 7).

The relative number of breakages and DSD of each type of breakages

The contributions of each type of breakages (i.e., binary, ternary and quaternary breakages) to the overall breakages can be evaluated from the relative breakage numbers, that is, $\Omega_2(V_0)/\Omega(V_0)$, $\Omega_3(V_0)/\Omega(V_0)$, and $\Omega_4(V_0)/\Omega(V_0)$. The breakage frequency density functions $\Omega_2(V_0)$, $\Omega_3(V_0)$, $\Omega_4(V_0)$, and $\Omega(V_0)$ can be calculated by Eqs. 29, 31, 33, and 34, respectively. Figure 9 shows the comparison of the predicted relative numbers and the experimental data. Maaß et al.[50] performed the single droplet breakage experiments in a breakage cell. The cell seems to be the same device used by Maaß et al.[10] The statistical significance of the analyzed data set was always tested by cumulative averaging of the observed results over the number of breakage events. Thus, the experimental data in the case of the maximal recorded amount of breakage events are chose to test the predicted values. That is, petroleum droplet of size 1.9 mm and toluene droplet of size 3.0 mm. In these conditions, the amount of the recorded breakage events of each size was over 780, and the statistical significance seems to be satisfied. In the experiments of Maaß et al.,[50] the pictures of the single droplet breakage event and the resulting daughter droplets were taken with a high-speed camera using a frame rate of 822 fps.

As seen from Figure 9, the measured values of petroleum droplet of size 1.9 mm are very close to those of toluene droplet of size 3.0 mm. That is, the relative numbers of binary, ternary and quaternary breakages are about 0.74, 0.19, and 0.07, respectively, in the conditions shown in Figure 9. Note that the probability of breakages of forming

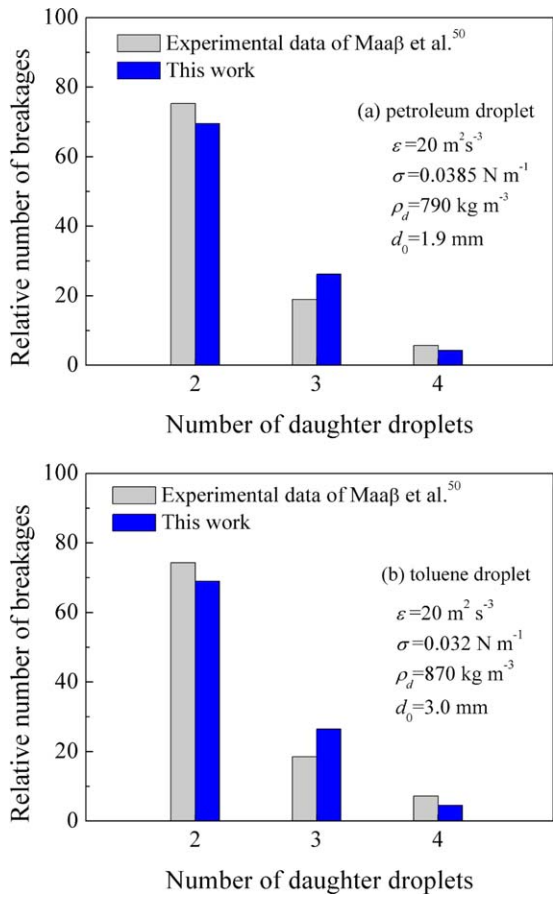

Figure 9. Comparison of the predicted relative number of breakages and the experimental data.

[Color figure can be viewed in the online issue, which is available at wileyonlinelibrary.com.]

more four daughter droplets is less than 0.02, and the method for estimating the turbulent dissipation rate will be given in the next section. The predicted results show an agreement with the experimental trend. Andersson and Andersson[21] also measured the probabilities of binary, ternary and quaternary breakages in turbulent flows. The relative numbers of binary, ternary and quaternary breakages are about 0.49, 0.33, and 0.18, respectively, in the condition of ε=8.5 m^2 s^{-3} (the overall probability of binary, ternary, and quaternary breakages is about 0.83). However, the amount of investigated events was not given by them. Thus, whether the statistical significance is satisfied is not known. In addition, the sizes of droplets were also not given. The experimental results of the relative number of breakages are not compared with the predicted results.

It should be pointed out that the measured data of the relative number of breakages seem to be related with the frame rate of the used camera in some extent. Maaß et al.[50] found that the relative number of binary breakage events decreases with the decreasing frame rate. For example, when the frame rate decreases from 822 to 125 fps, the probability of binary breakage decreases from 0.74 to 0.45. The frame rate of 125 fps may be too low since its time resolution is about 8 ms while the arithmetic average breakage times of petroleum droplet of 1.9 mm and toluene droplet of size 3.0 mm are about 13.9 and 16.1 ms, respectively, in the experiments of Maaß et al.[50] with 822 fps. The time resolution of 822 fps is about 1.2 ms.

To discuss the DSD separately for the binary, ternary and quaternary breakages, the DSD probability density function with respect to a general daughter size fraction f_v (i.e., $\beta_n(f_v, V_0)$) is defined as follows

$$\beta_n(f_v, V_0) = \frac{\varphi_n(f_v, V_0)}{\int_0^1 \varphi_n(f_v, V_0) df_v} \tag{36}$$

where, n=2, 3, 4. $\beta_n(f_v, V_0)$ denotes the contribution of the breakage events that at least one of the volumes of daughter droplets equals to $V(=f_v V_0)$. $\varphi_2(f_v, V_0)$, $\varphi_3(f_v, V_0)$, and $\varphi_4(f_v, V_0)$ are calculated by Eqs. 28, 30, and 32, respectively.

For ternary breakage (n=3) and quaternary breakage (n=4), $\beta_n(f_v, V_0)$ can also be written as follows

$$\beta_n(f_v, V_0) = \sum_{i=1}^{n-1} \beta_{n,i}(f_{v,i} = f_v, V_0) \tag{37}$$

where, i=1, 2, 3, and

$$\beta_{n,i}(f_{v,i} = f_v, V_0) = \frac{\varphi_{n,i}(f_{v,\ i} = f_v, V_0)}{\int_0^1 \varphi_n(f_v, V_0) df_v} \tag{38}$$

$$\varphi_{3,1}(f_{v,1} = f_v, V_0) = \frac{1}{2}\int_0^{1-f_v} \phi_3 df_{v,2} \tag{39}$$

$$\varphi_{3,2}(f_{v,2} = f_v, V_0) = \int_0^{1-f_v} \phi_3 df_{v,1} \tag{40}$$

$$\varphi_{4,1}(f_{v,1} = f_v, V_0) = \int_0^{1-f_v} \int_0^{1-f_v-f_{v,2}} \frac{\phi_4}{2} df_{v,3} df_{v,2} \tag{41}$$

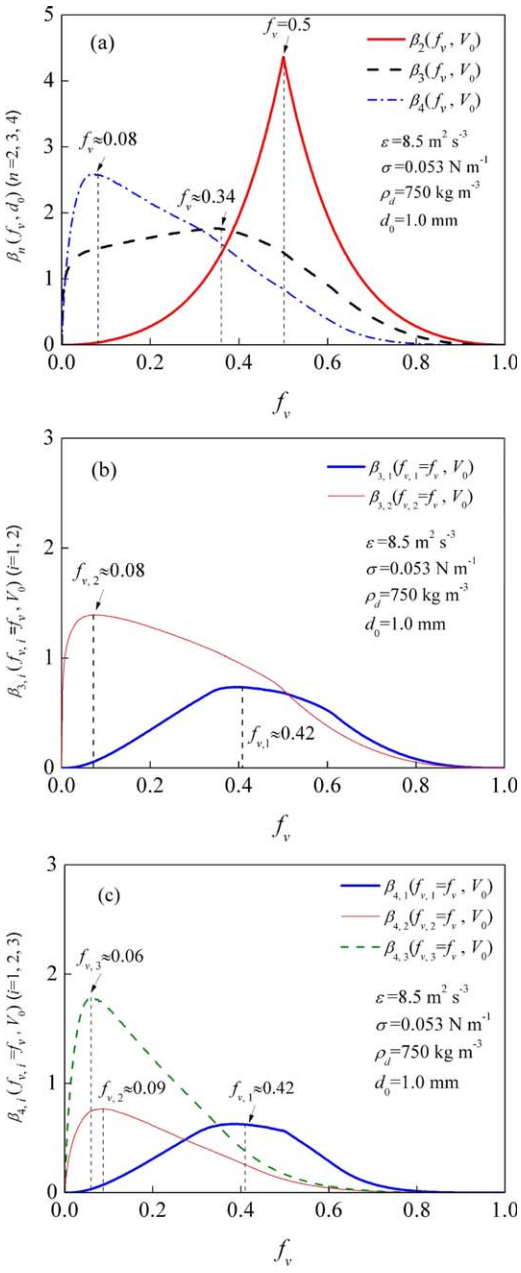

Figure 10. $\beta_n(f_v, d_0)$ or $\beta_{n,i}$ ($f_{v,i}=f_v$, d_0) vs. f_v.

[Color figure can be viewed in the online issue, which is available at wileyonlinelibrary.com.]

$$\varphi_{4,2}(f_{v,2} = f_v, V_0) = \int_0^{1-f_v} \int_0^{1-f_v-f_{v,1}} \frac{\phi_4}{2} df_{v,3} df_{v,1} \tag{42}$$

$$\varphi_{4,3}(f_{v,\ 3} = f_v, V_0) = \int_0^{1-f_v} \int_0^{1-f_v-f_{v,1}} \phi_4 df_{v,2} df_{v,1} \tag{43}$$

Figure 10a shows $\beta_2(f_v, V_0)$, $\beta_3(f_v, V_0)$, and $\beta_4(f_v, V_0)$. It can be seen that the probability of equal-sized breakage is the maximal for binary breakage of droplet, while the unequal-sized breakage is the most possible in the cases of ternary and quaternary breakages. Note that $\beta_3(f_v, V_0)$ reaches a peak value when f_v is about 0.34 for ternary breakage. But it may not indicate that the probability of forming three daughter droplets of similar sizes (i.e., $f_{v,1}$=0.34, $f_{v,2}$=0.34, and $f_{v,3}$=0.32) is the maximal. This is because

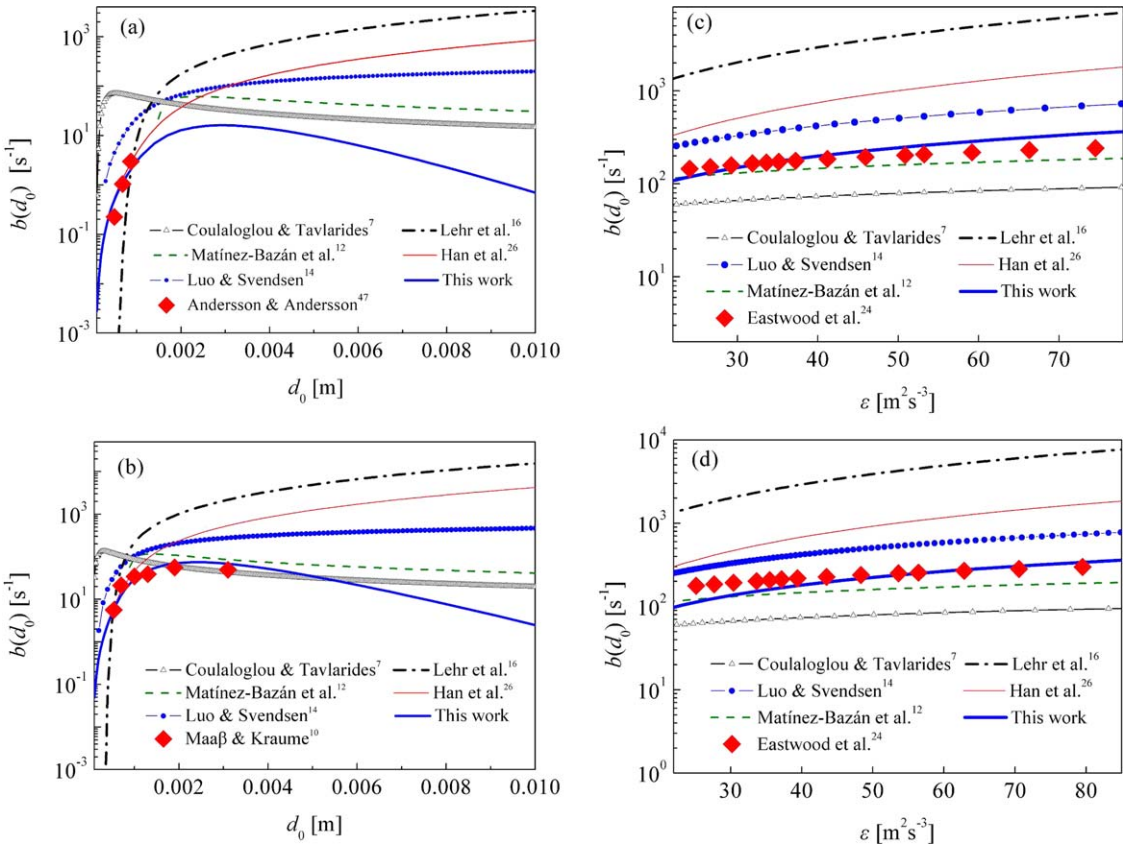

Figure 11. Comparison of the results predicted by different breakage frequency models and the experimental data.

(a) Dodecane water system (ε=8.5m^2 s^{-3}, μ_c=0.001 Pa s, μ_d=0.0015 Pa s, ρ_c=1000 kg m^{-3}, ρ_d=750 kg m^{-3}, σ=0.053 N m^{-1}, Oh<0.01, θ_{min}<0.01); (b) petroleum water system (ε=20m^2 s^{-3}, μ_c=0.001 Pa s, μ_d=0.00065 Pa s, ρ_c=1000 kg m^{-3}, ρ_d=790 kg m^{-3}, σ=0.0385 N m^{-1}, Oh<0.005, θ_{min}<0.0012); (c) silicone oil water system (d_0=1.92 mm, μ_c=0.001 Pa s, μ_d=0.0052 Pa s, ρ_c=1000 kg m^{-3}, ρ_d=918 kg m^{-3}, σ=0.033 N m^{-1}, Oh<0.02, θ_{min}<0.00012); and (d) silicone oil water system (d_0=1.93 mm, μ_c=0.001 Pa s, μ_d=0.0097 Pa s, ρ_c=1000 kg m^{-3}, ρ_d=936 kg m^{-3}, σ=0.035 N m^{-1}, Oh<0.04, θ_{min}<0.00012). [Color figure can be viewed in the online issue, which is available at wileyonlinelibrary.com.]

three different types of breakages contribute to the peak value of $\beta_3(f_v, V_0)$. That is, $f_{v,1}$=0.34, $f_{v,2}$=0.34, and $f_{v,1}$=0.34 & $f_{v,2}$=0.34. When $f_{v,1}$=0.34, $f_{v,2}$ can vary from 0 to 0.66, and when $f_{v,2}$=0.34, $f_{v,1}$ can also vary from 0 to 0.66. Thus, there are many other possible events in the first and second breakage types contributing to the peak value. The breakage of $f_{v,1}$=0.34, $f_{v,2}$=0.34, and $f_{v,3}$=0.32 is only one type of the possible events contributing to this peak value.

The most possible breakages in the case of ternary breakage can be evaluated from the breakages represented by the most possible size fractions of daughter droplets of sizes d_1 and d_2 shown in Figure 3b according to the peak values of $\beta_{3,1}(f_{v,1}=f_v, V_0)$ and $\beta_{3,2}(f_{v,2}=f_v, V_0)$. It can be seen from Figure 10b that $\beta_{3,1}(f_{v,1}=f_v, V_0)$ has a maximum when $f_v(=f_{v,1})\approx 0.42$. It means that the probability of forming daughter droplet of size fraction $f_{v,1}\approx 0.42$ is the maximal. On the other hand, $\beta_{3,2}(f_{v,2}=f_v, V_0)$ has a maximum when f_v $(=f_{v,2})\approx 0.08$. That is, the probability of forming daughter droplet of size fraction $f_{v,2}\approx 0.08$ is the maximal. Thus, as a whole, the probability of the breakages denoted by $f_{v,1}\approx 0.42$, $f_{v,2}\approx 0.08$, and $f_{v,3}\approx 0.5$, namely, the probability of forming two daughter droplets of comparable sizes and one daughter droplet of small size, is the maximal for ternary breakage of low viscous droplets.

As seen from Figure 10a, $\beta_4(f_v, V_0)$ has a peak value when f_v is about 0.08. This peak value seems not to directly account for the most possible breakages as there are seven different breakage types contributing to this peak value. The possible breakages in quaternary case can be evaluated from the breakages represented by the possible size fractions of daughter droplets of d_1, d_2, and d_3 according to the peak values of $\beta_{4,1}(f_{v,1}=f_v, V_0)$, $\beta_{4,2}(f_{v,2}=f_v, V_0)$, and $\beta_{4,3}(f_{v,3}=f_v, V_0)$. It can be seen from Figure 10c that $\beta_{4,1}(f_{v,1}=f_v, V_0)$ has a maximum when f_v $(=f_{v,1})\approx 0.42$, $\beta_{4,2}(f_{v,2}=f_v, V_0)$ has a maximum when f_v $(=f_{v,2})\approx 0.09$, $\beta_{4,3}(f_{v,3}=f_v, V_0)$ has a maximum when f_v $(=f_{v,3})\approx 0.06$. Thus, as a whole, the probability of the breakages denoted by $f_{v,1}\approx 0.42$, & $f_{v,2}\approx 0.09$, and $f_{v,3}\approx 0.06$ & $f_{v,4}\approx 0.43$, namely, the probability of forming two daughter droplets of comparable sizes and two daughter droplets of small sizes, seems to be the maximal for quaternary breakage of low viscous droplets.

Comparison with the experimental data and other models: Breakage frequency

As shown in Figures 11a,b, the breakage frequencies predicted by the models of Coulaloglou and Tavlarides[7] and Martínez-Bazán et al.[12] exhibit a nonmonotonic trend with increasing d_0, while the breakage frequencies predicted by the models of Luo and Svendsen,[14] Lehr et al.,[16] and Han et al.[26] monotonously increase with d_0. The breakage frequencies predicted by the model of Han et al.[26] can give a good agreement with the experimental data when d_0 is smaller than about 1.0 mm, however, it predicts the much higher breakage frequencies than the

experimental data when d_0 is larger than about 1.0 mm. The model proposed by Coulaloglou and Tavlarides[7] has been widely used to predict droplet breakage in liquid–liquid system, and the values of two unknown model parameters given by them were also used in this work (i.e., C_1=0.336, C_2=0.106). The models of Luo and Svendsen[14] and Martínez-Bazán et al.[12] seem to overestimate the breakage frequencies as a whole. Furthermore, the breakage will not occur according to the model of Martínez-Bazán et al.[12] (i.e., the breakage frequency will be negative) when d_0 is smaller than about 1.5 mm in Figure 11a or smaller than about 0.85 mm in Figure 11b. It should be pointed out that the volume fraction α_d of dispersed phase appearing in Eqs. 25 and 26 is neglected since α_d is very low in the case of the single droplet experiments.

In Figure 11a, the experimental data of Andersson and Andersson[47] were measured from a fully developed turbulent flow, where the breakage experiments of dodecane droplets of size smaller than about 1.0 mm were performed in the condition of ε=8.5 m^2 s^{-3}. Maaβ and Kraume[10] also measured the breakage frequencies in a breakage cell. As mentioned before, this cell was used to represent the turbulent flow near the impeller blade. It should be noted that the turbulent dissipation rate in their experiments was not given, which could be estimated from the relationship, $\varepsilon_i \approx 4.0 N_{im}^2 D_{im}^2$. Here, ε_i is mean turbulent dissipation rate near the impeller blade, $N_{\rm im}$ is the speed of impeller and $D_{\rm im}$ is the diameter of impeller. This relationship was estimated by Han et al.[44] according to the experimental studies of Escudié and Liné[51] and Baldi and Yianneskis,[52] then $\varepsilon_i \approx$20.0 m^2 s^{-3}. Maaβ and Kraume[10] proposed a β-distribution of breakage time to remove the effect of high circulation time caused by the process of large eddies catching droplets. However, the arithmetic mean of breakage time was still used to calculate the breakage frequency in this work, since the effect of large eddies on breakage has been considered in the proposed model. As seen from Figures 9a,b, the experimental data of Andersson and Andersson[47] showed that the breakage frequency increases with increasing d_0 when d_0 is smaller than about 1.0mm. This trend was also shown by the experimental data of Maaβ and Kraume.[10] But Maaβ and Kraume[10] further found that the breakage frequency increases to a maximum and then decreases with increasing d_0. As a whole, the proposed model (i.e., Eqs. 27–34 coupled with Eq. 7) gives a reasonable agreement with the experimental data since this model considers the effect of the wide energy spectrum distribution.

As seen from Figures 11c,d, the breakage frequencies predicted by the above breakage models exhibit a monotone increase with turbulent dissipation rate ε. Nevertheless, the models of Coulaloglou and Tavlarides[7] and Martínez-Bazán et al.[12] seem to underestimate the breakage frequencies as a whole, and the models of Luo and Svendsen,[14] Lehr et al.,[16] and Han et al.[26] obviously overestimate the breakage frequencies. The results predicted by the proposed model show a better agreement with the experimental data of Eastwood et al.[24] (in which, α_d was about 0.2–1.2%) in comparison with those predicted by other models as a whole. Notice that the breakage frequencies predicted by the model of Prince and Blanch[11] are not shown in Figure 9 since these results are much higher than the experimental data.

Comparison with the experimental data and other models: DSD

Zaccone et al.[22] measured the diameter-based DSDs for binary, ternary, and quaternary breakages of petroleum droplets in a breakage cell. It should be pointed out that the breakage cell and the operating conditions in both of the experiments of Zaccone et al.[22] and Maaß and Kraume[10] seem to be the same. Thus, the mean turbulent dissipation rate near impeller blade will be used for the simulation of DSD. Zaccone et al.[22] recorded large numbers of single droplet breakage events, and then assigned the recorded diameters of all the daughter droplets after each breakage to the corresponding size intervals, where the region of (0, d_0) was divided into many equal intervals. To make the predicted distributions comparable with the experimental data, the following dimensionless diameter-based DSD function is defined

$$\beta_n(f_{\rm d}, d_0) = \frac{b_n(f_{\rm d}, d_0)}{\int_0^1 b_n(f_{\rm d}, d_0) df_{\rm d}} \tag{44}$$

where n=2, 3, 4, $f_{\rm d}$=d/d_0, $b_n(f_{\rm d}, d_0)$ is diameter-based function representing the breakage in which at least one of size fractions of the daughter droplets equals to $f_{\rm d}$. $b_n(f_{\rm d}, d_0)$ is calculated from volume-based function of $\varphi_n(f_{\rm v}, V_0)$, but the integrals are about $f_{\rm d}$ and all the variables of $f_{\rm v}$ and $f_{{\rm v},j}$ (j=1, 2, 3, l) appearing in the integrand of ϕ_n are substituted by f_d^3 and $f_{d,j}^3$, and the integral upper limits of $1-f_{\rm v}$ and $1-f_{\rm v}-f_{{\rm v},l}$ are substituted by $(1-f_d^3)^{1/3}$ and $(1-f_d^3-f_{d,l}^3)^{1/3}$, respectively. The factor 1/2 appearing in $\varphi_n(f_{\rm v}, V_0)$ is not included in $b_n(f_{\rm d}, d_0)$ as $\beta_2(f_{\rm d}, d_0)$, $\beta_3(f_{\rm d}, d_0)$, and $\beta_4(f_{\rm d}, d_0)$ are unsymmetrical with a certain $f_{\rm d}$ when $f_{\rm d}$ ranges from 0 to 1. The function $b_n(f_{\rm d}, d_0)$ represents the probability density for formation of droplets within the interval between $f_{\rm d}$ and $f_{\rm d}+df_{\rm d}$. The volume-based function of Luo and Svendsen[14] could be transformed into the diameter-based type using the method similar to Eq. 44.

In the literature, there are several DSD models for binary, ternary and quaternary breakages, respectively. The model of Coulaloglou and Tavlarides,[7] Luo and Svendsen,[14] and Martínez-Bazán et al.[13] can predict DSD of binary breakage, the DSD of ternary breakage can be predicted by the model of Konno et al.[23] and Martínez-Bazán et al.[13] The model of Diemer and Olson[28] containing an unknown parameter q can be used to predict the DSD of binary, ternary and quaternary breakages, simultaneously. To make the profile trend of diameter-based DSD similar to that of volume-based DSD (e.g., $f_{\rm d}\to 0$ and $f_{\rm v}\to 0$, the DSD will tend to zero), the model parameter q is taken as 4, 1.5, and 1.4 for binary, ternary, and quaternary breakages, respectively.

As shown in Figure 12a, the proposed model predicts a maximal probability of equal-sized binary breakage, and the DSD tends to 0 when $f_{\rm d}\to 0$ or 1. Moreover, the trend predicted by the proposed model seems consistent with experimental data as a whole. The model of Luo and Svendsen[14] predicts a maximal probability of unequal-sized binary breakage, while the models of Coulaloglou and Tavlarides,[7] Martínez-Bazán et al.,[13] and Diemer and Olson[28] can also predict a maximal probability of equal-sized breakage, but the maximum seems much higher than or much smaller than the experimental data. Notice that the DSD model of Martínez-Bazán et al.[13] was derived from the breakage of gas bubbles, but it has also been applied to liquid–liquid systems in recent years.

For ternary breakage, Martínez-Bazán et al.[13] assumed that a fluid particle breaks into one daughter fluid particle and other two identical daughter fluid particles. The proposed model is compared with the experimental data and the models of Konno et al.,[23] Martínez-Bazán et al.,[13] and

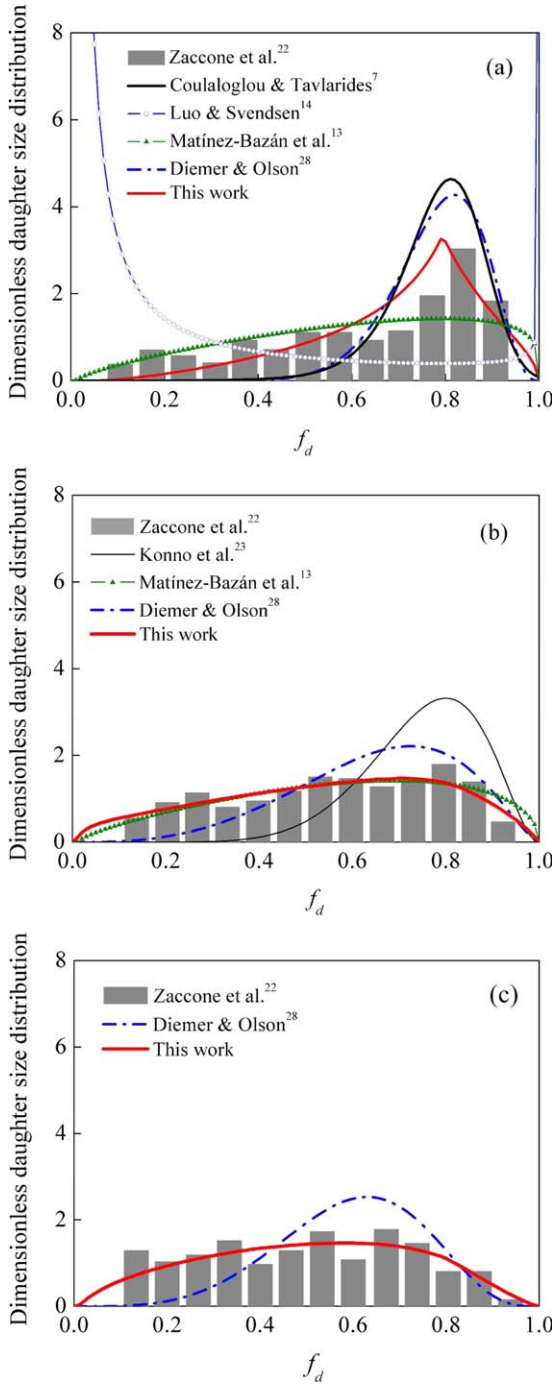

Figure 12. Comparison of the results predicted by different DSD models and the experimental data ($f_d=d/d_0$, ε=20 m^2 s^{-3}, μ_c=0.001 Pa s, μ_d=0.0019 Pa s, ρ_c=1000 kg m^{-3}, ρ_d=760 kg m^{-3}, σ=0.002 N m^{-1}, Oh<0.05, θ_{min}<0.0012).

(a) Binary breakage; (b) ternary breakage; and (c) quaternary breakage. [Color figure can be viewed in the online issue, which is available at wileyonlinelibrary.com.]

Diemer and Olson[28] (please see Figure 12b). The DSD predicted by the model of Konno et al.[22] nearly tends to 0 when f_d is smaller than about 0.38, and the model of Diemer and Olson[27] gives the similar trend when f_d is smaller than about 0.16. The models of Konno et al.[23] and Diemer and Olson[28] predict much higher peak values and the narrower profiles of DSD in comparison with the experimental data. The model of Konno et al.[23] does not contain any unknown parameter and can be applied directly. The distribution predicted by this model appears explicitly independent on the underlying turbulence and the surface tension. The model of Martínez-Bazán et al.[13] and the proposed model predict a maximal probability of forming one daughter droplet of small size and other two large droplets of comparable sizes (i.e., $f_d\approx0.73$).

For quaternary breakage, the proposed model is compared with the experimental data and the model of Diemer and Olson[28] in Figure 12c. The model of Diemer and Olson[28] predicts a maximal probability of equal-sized breakage (i.e., $f_d\approx0.63$), and the predicted profiles obviously underestimate the distribution when $f_d<0.3$. The proposed model predicts a quite even distribution when f_d varies from 0 to 1, which shows a reasonable agreement with the trend given by the experimental data of Zaccone et al.[22]

It should be pointed out that the other process for quaternary breakage is also likely. Namely, after parent droplet becomes a complex and deformed body, the body is likely split into two intermediates of equivalent sizes $d_{In,1}$ and $d_{In,2}$ first, and then one of them ($d_{In,1}$) breaks into two daughter droplets of sizes d_1 and d_2, the other ($d_{In,2}$) breaks into two daughter droplets of sizes d_3 and d_4. The breakage constraint of this process is somewhat different from the constraint of Eqs. 19 and 20, namely

$$\begin{aligned} D_{ke} \geq & \left[\max\left(D_{se,In,1}, D_{se,In,2}\right) - D_{se,0}\right] \\ & + \left[\max\left(D_{se,1}, D_{se,2}\right) - D_{se,In,1}\right] \\ & + \left[\max\left(D_{se,3}, D_{se,4}\right) - D_{se,In,2}\right] \end{aligned} \tag{45}$$

$$\begin{aligned} e(k) \geq \pi d_0^2\sigma\{ & \{\max[(f_{v,1}+f_{v,2})^{-1/3}, (f_{v,3}+f_{v,4})^{-1/3}] - S_d\} \\ & + C_q^*[\max({f_{v,1}}^{-1/3}, {f_{v,2}}^{-1/3}) - (f_{v,1}+f_{v,2})^{-1/3} \\ & + \max({f_{v,3}}^{-1/3}, {f_{v,4}}^{-1/3}) - (f_{v,3}+f_{v,4})^{-1/3}]\} \end{aligned} \tag{46}$$

where $S_d = S/\left(\pi d_0^2\sigma\right)$, $f_{v,4}=1-f_{v,1}-f_{v,2}-f_{v,3}$.

Note that in the above breakage process, the daughter droplets of sizes d_1 and d_2 (or d_3 and d_4) are statistically indistinguishable each other since they are formed by the same process, d_1 and d_3 are statistically distinguishable each other, d_1 and d_2 can be statistically exchanged with d_3 and d_4 as a whole since they are formed by the similar process. Thus, unlike Eqs. 32 and 33, $\varphi_4(f_v, V_0)$ is calculated by $\int_0^{1-f_v}\int_0^{1-f_v-f_{v,2}} (\phi_4/2)df_{v,3}df_{v,2}$(where the factor 1/2 takes into account that the integrand ϕ_4 is symmetrical with $f_{v,3}=(1-f_{v,1}-f_{v,2})/2$ since the size fractions of $f_{v,3}$ and $f_{v,4}$ are statistically exchangeable each other) and $\Omega_4(V_0)$ is calculated by $\left(\int_0^1 \varphi_4\left(f_v, V_0\right)df_v\right)/2$ (where the factor 1/2 takes into account that the breakages will be counted twice when overall frequency $\Omega_4(V_0)$ is calculated). The diameter-based DSD is calculated by Eq. 44, but $b_4(f_d, d_0)$ appearing in this equation is calculated by $\int_0^{(1-f_d^3)^{1/3}}\int_0^{(1-f_d^3-f_{d,2}^3)^{1/3}} (\phi_4/2)df_{d,3}df_{d,2}$, ϕ_4 is calculated by Eq. 27.

Furthermore, we find that the breakage frequencies and DSDs predicted by Eqs. 33 and 44 adopting the two constraints (i.e., Eqs. 20 and 46) are close in values each other when C_q* and C_q (appearing in Eq. 20) are taken as two comparable values, that is, 0.08 and 0.11, respectively.

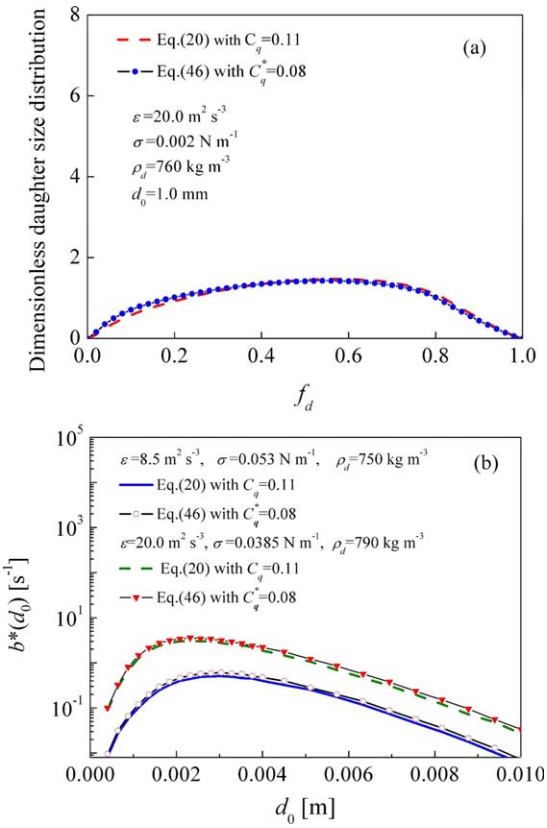

Figure 13. Effect of two different processes on DSD and breakage frequency for quaternary breakage (μ_c=0.001 Pa s, ρ_c=1000 kg m^{-3}).

[Color figure can be viewed in the online issue, which is available at wileyonlinelibrary.com.]

Please see the example shown in Figure 13. It implies that the two constraints have the similar effects on the breakage frequencies and DSDs when parent droplet experiences a full deformation. Thus, in this work, we adopt the constraint of Eq. 20 to model the quaternary breakage.

Comparison with the experimental data and other models: PBE

To our knowledge, there are two methods to validate the breakage models in the literature. The one is the direct comparison of the predicted breakage frequency or DSD with the experimental data. The other is to couple the breakage model with PBE to predict the evolution of size distribution of droplets. The first method has been adopted in the above sections, now the second method will be used to further test the proposed model.

Konno et al.[23] measured the cumulative size distributions of water o-xylene-CCl_4 system in a stirred tank with a Rushton turbine, and α_d was kept below 0.2%. Therefore, the evolution of size distribution of droplets can be predicted by the breakage model coupled with PBE since α_d is very low and the coalescence of droplets can be neglected. Then, the PBE can be simplified as

$$\frac{\partial n(V,t)}{\partial t}=\int_{\Sigma_V} m(V_0)\beta'(V,V_0)\Omega(V_0)n(V_0,t)dV_0-\Omega(V)n(V,t) \tag{47}$$

where $n(V, t)$ is the number of droplets of volume V at a given time t, $m(V_0)$ is the mean number of daughter droplets, and $m(V_0)\beta'(V,V_0)$ is called the redistribution probability function.[5] Notice that $m(V_0)\beta'(V,V_0)$ can be obtained by $\beta(f_v,V_0)/V_0$, here $\beta(f_v, V_0)$ is given by Eq. 35, $\Omega(V_0)$ and $\Omega(V)$ are obtained by Eq. 34. According to Kumar and Ramkrishna,[53] Eq. 47 can be written as

$$\frac{dN_i(t)}{dt}=\sum_{k=i}^{M}T_{i,k}\Omega_k N_k(t)-\Omega_i N_i(t) \tag{48}$$

$$T_{i,k}=\int_{x_i}^{x_{i+1}}\frac{x_{i+1}-V}{x_{i+1}-x_i}\beta'(V,x_k)dV+\int_{x_{i-1}}^{x_i}\frac{V-x_{i-1}}{x_i-x_{i-1}}\beta'(V,x_k)dV \tag{49}$$

where, i denotes the ith size group of droplets, $N_i(t)=\int_{V_i}^{V_{i+1}}n(V,t)dV$, Eq. 48 can be solved by numerical method of Runge-Kutta.

Moreover, the mean number of daughter droplets could be obtained from the mass conservation of multiple breakages. That is

$$m(V_0)\int_0^1 f_v\beta(f_v,V_0)df_v=1 \tag{50}$$

In Figure 14, the experimental data at 0.5 min are used as the initial condition, and the sizes of droplets (ca. 10–300 μm) are divided into 61 size groups for PBE. In Figure 15, the experimental data at 3.0 min are used as the initial condition, and the sizes of droplets (ca. 10–500 μm) are also divided into 61 size groups for PBE.

Note that, in stirred tank, the turbulence level in the discharge flow region (including the region close to impeller in this work) is usually much higher than that in the circulation flow region. The turbulence in the discharge flow region may be mainly responsible for the breakage of droplets.[8] Therefore, the turbulent dissipation rate in this region needs to be used for PBE. We adopt the relation given by Placek and Tavlarides,[54] $\varepsilon_d/\varepsilon_m\approx5.16$ for $D_{im}/D_T=1/2$, to estimate the mean turbulent dissipation rate ε_d in the discharge flow region. Here, ε_m denotes the mean turbulent dissipation rate over the whole stirred tank. This relation was also adopted by Tsouris andTavlarides.[8] In the experiment of Konno et al.[23] (D_T=0.3 m, μ_c=0.001 Pa s, ρ_c=1000 kg m^{-3}, ρ_d=1040 kg m^{-3}, σ=0.034 N m^{-1}), $\varepsilon_m\approx1.6$ m^2 s^{-3} when N_{im}=257 rpm in Figure 14 and $\varepsilon_m\approx0.22$ m^2 s^{-3} when N_{im}=131 rpm in Figure 15.

Notice that the relation of $\varepsilon_i\approx4.0N_{im}^2D_{im}^2$ mentioned before seems not suitable to these cases since the discharge flow region is much wider than the region near the impeller blade. As mentioned before, in the experiment of Maaß and Kraume,[10] the breakage cell was mainly used to represent the turbulent flow close to impeller blade.

Figures 14 and 15 show the comparison of the predicted cumulative volume fraction distributions (i.e., $F(V,t)=\int_{V_{min}}^{V}vn(v,t)dv$, v denotes the volume of droplet in the region of (V_{min}, V), $V\le V_{max}$) and the experimental data of Konno et al.[23] As a whole, the model of Luo and Svendsen[14] underestimate the distributions. But for the droplets of small size, the model of Luo and Svendsen[14] seems to overestimate the distributions. Notice that, the original lower and upper integral limits in the model of Luo and Svendsen[14] are $11.4\eta\sim31.4\eta$ and d_0, respectively. But it means that the breakage frequency may be negative since the droplets of size d_0 (10–300 μm in Figure 10 and 14−500 μm in Figure 15) are quite likely smaller than the eddies of size

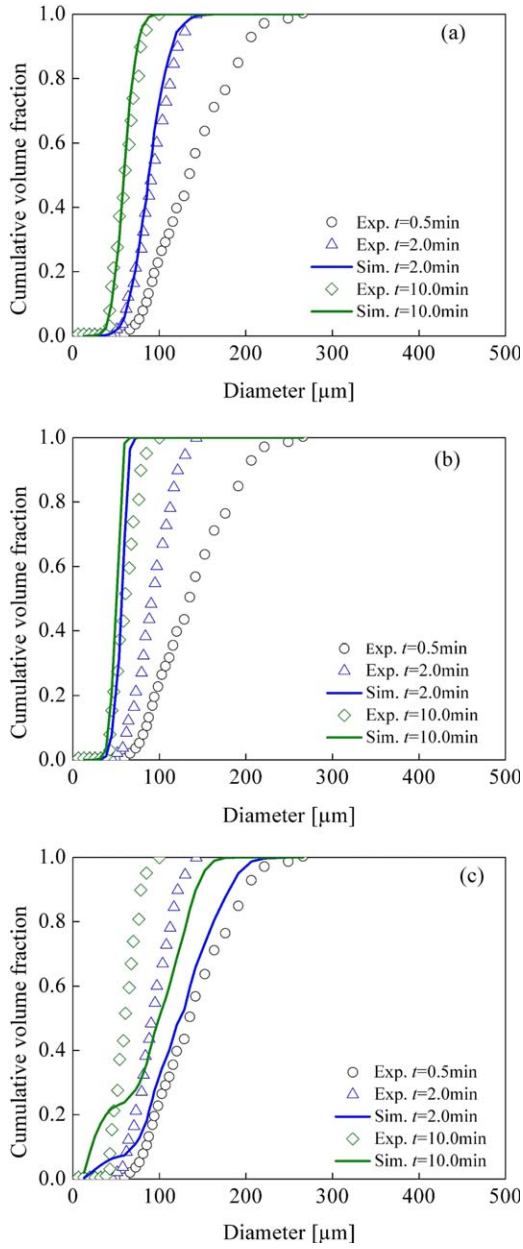

Figure 14. Comparison of the cumulative volume fraction predicted by different models and the experimental data of Konno et al.[23] (ε_d=8.26m^2 s^{-3}, μ_c=0.001 Pa s, μ_d=0.0008 Pa s, ρ_c=1000 kg m^{-3}, ρ_d=1040 kg m^{-3}, σ=0034 N m^{-1}, D_T=0.3 m, N_{im}=257 rpm, Oh<0.04, θ_{min}<0.0008).

(a) This work; (b) the model of Coulaloglou and Tavlarides[7]; and (c) the model of Luo and Svendsen.[14] [Color figure can be viewed in the online issue, which is available at wileyonlinelibrary.com.]

$11.4\eta-31.4\eta$ (i.e., 213–586 μm in Figure 14 and 349–961 μm in Figure 15) Thus, the lower integral limit for the model of Luo and Svendsen[14] is adjusted as η ($\eta\approx$18.7 μm in Figure 14 and $\eta\approx$30.6 μm in Figure 15).

It should be pointed out that, in Figures 14b and 15b, the original values of C_1 and C_2 in the model of Coulaloglou and Tavlarides[7] are used. In PBE, $\beta'(V,V_0)$ proposed by Coulaloglou and Tavlarides,[7] that is, $2.4\exp(-4.5(2V-V_0)^2/V_0^2)/V_0$ is coupled with their breakage frequency model. As shown in Figures14 and 15, the cumulative volume fractions predicted by the proposed model show an agreement with the experimental data. As a whole, the model of Luo and Svendsen[13] underestimates the breakage frequencies of droplets for the experiment system of Konno et al.,[23] therefore, the cumulative volume fraction predicted by this model is also underestimated. But the model of Coulaloglou and

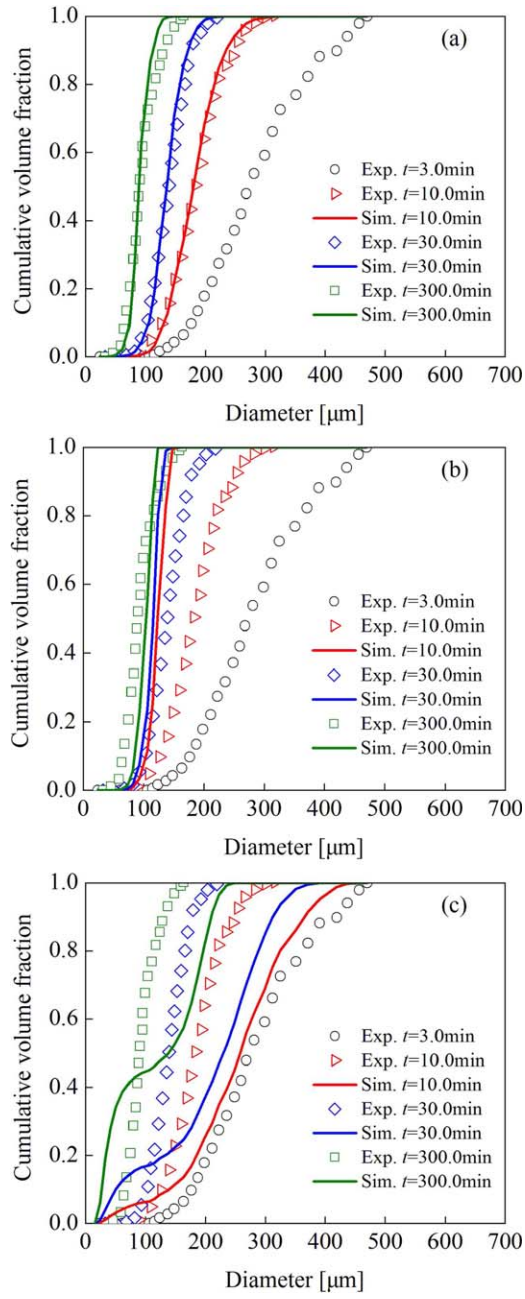

Figure 15. Comparison of the cumulative volume fraction predicted by different models and the experimental data of Konno et al.[22] (ε_d=1.14 m^2 s^{-3}, μ_c=0.001 Pa s, μ_d=0.0008 Pa s, ρ_c=1000 kg m^{-3}, ρ_d=1040 kg m^{-3}, σ=0.034 N m^{-1}, D_T=0.3 m, N_{im}=131 rpm, Oh<0.04, θ_{min}<0.0013).

(a) This work; (b) the model of Coulaloglou and Tavlarides[7]; and (c) the model of Luo and Svendsen.[14] [Color figure can be viewed in the online issue, which is available at wileyonlinelibrary.com.]

Tavlarides[7] seems to overestimate the cumulative volume fraction when $t<30.0$min. The results predicted by the models of Matínez-Bazán et al.,[12,13] Lehr et al.,[16] and Zhao and Ge[19] are not shown in Figures 14 and 15 as the predicted breakage frequencies are very low or negative in the experimental conditions of Konno et al.[23]

Conclusions

An improved mathematical model for multiple breakages (i.e., the main binary, ternary and quaternary breakages) of low viscous droplets has been developed, which can be coupled with the wide energy spectrum (i.e., Eq. 7). In this model, the effects of the underlying turbulence, the parent droplet size, the energy spectrum distribution on breakage frequency and DSD were considered. Furthermore, the surface oscillation resulting from the previous interactions between the droplet and the eddy has been considered. An analytical expression for estimating the surface oscillation was presented to describe the mean shape of parent droplet based on the interaction forces (e.g., the turbulent fluctuation pressure and surface tension force) between the droplet and the surrounding fluid. The effect of this oscillation on the constraints of multiple breakages and the collision frequency density has also been accounted for in this work.

The wide energy spectrum distribution was found to have an important effect on the nonmonotone behavior of breakage frequency with increasing d_0. The wide energy spectrum can distinguish the dissipation range, the inertia subrange and the energy containing range. The breakage frequency predicted by the proposed model coupled with the wide energy spectrum increases to a maximum and then decreases with increasing d_0. While ESIS will monotonously increase with decreasing k when it is used to cover the size range of eddies contributing to the breakage (i.e., $\lambda \geq 11.4$–31.4η, this method was usually adopted by the previous models). The breakage frequency predicted by the proposed model coupled with ESIS monotonously increases with increasing d_0.

As a whole, the breakage frequencies predicted by this model coupled with the wide energy spectrum showed a good agreement with the experimental data of Maaβ and Kraume,[10] Eastwood et al.,[24] and Andersson and Andersson.[47] Furthermore, the DSDs of binary, ternary and quaternary breakages predicted by the proposed model can give a relatively reasonable agreement with the experimental data of Zaccone et al.[22] The cumulative volume fractions predicted by PBE coupled with this model also showed a good agreement with the experimental data of Konno et al.[23] as a whole.

Further work, such as the effect of viscosity of dispersed phase should be considered for high viscous system and the turbulence structure of energy containing range should be studied in depth, and the improved experimental studies are also needed.

Acknowledgments

The authors acknowledge the financial support from the National Natural Science Foundation of China (21106122, 21176204, and 21376198), the scientific research fund of Hunan Provincial Education Department (11B123), and the Hunan Provincial Innovation Foundation for Postgraduate (CX2013B273).

Notation

A = velocity amplitude of eddy, m s^{-1}
A_x = amplitude of surface oscillation, m
a, b = semiaxses of an ellipsoidal droplet, m
a', b' = semiaxses of an oval collision cross section, m
$b(d_0)$ = breakage frequency of droplet of size d_0, ($=\Omega(V_0)/ n_d$), s^{-1}
$b^*(d_0)$ = specific breakage frequency of droplet of size d_0, ($=\Omega(V_0)/ [(1-\alpha_d)n_d]$), s^{-1}
$bn(f_d, d_0)$ = diameter-based function representing the breakage of droplet with size d_0 at which at least one of size fractions of the daughter droplets equals to f_d
C = Kolmogorov constant
C_0, C_1, C_2, C_3 = coefficients
C_t = deformation factor of intermediate in ternary breakage
C_q = deformation factor of intermediate in quaternary breakage
D_{im} = diameter of impeller, m
D_{ke} = energy density of parent droplet, J m^{-3}
$D_{ke,critical}$ = critical energy density of parent droplet, J m^{-3}
$D_{se,0}$ = surface energy density of parent droplet, J m^{-3}
$D_{se,In}$ = surface energy density of intermediate in ternary or quaternary breakage, J m^{-3}
$D_{se,i}$ = surface energy density of daughter droplet i (i=1, 2, 3, 4), J m^{-3}
D_T = diameter of stirred tank, m
d = general diameter of droplet, m
d_0 = diameter of parent droplet, m
d_c = diameter of droplet having the maximal breakage frequency, m
d_{In},i = diameter of intermediate in ternary of quaternary breakage, m
d_i = diameter of daughter droplet (i=1, 2, 3, 4), m
$E(k)$ = the energy spectrum distribution function, m^2 s^{-3}
$e(d_0)$ = kinetic energy of parent droplet of size d_0, J
$e(k)$ = kinetic energy of eddy of wave number k, J
$e(\lambda)$ = kinetic energy of eddy of size λ, J
$e_{available}(k)$ = available energy of eddy of wave number k for breakage, J
$e_{critical},n$ = critical energy required for breakage of forming n daughter droplets, J
e_D = critical energy determined by the constraint of surface energy density increase, J
e_S = critical energy determined by the constraint of surface energy increase, J
$\bar{e}(k)$ = mean kinetic energy of eddy of wave number k, J
$\hat{e}k\sim k+dk$ = turbulent kinetic energy per unit mass contained in eddies of wave number between k and $k+dk$, J
$F(V, t)$ = cumulative volume fraction distribution
F_p = turbulent fluctuation pressure, N m$-^1$
f_v, f_d = general daughter droplet size factions, V/V_0 and d/d_0, respectively
f_v,i, f_d,i = daughter droplet size factions, V_i/V_0 and d_i/d_0 (i=1, 2, 3, 4), respectively
$f_{v,min}$, $f_{v,max}$ = the maximal and minimal daughter droplet size factions in the model of Wang et al.,[1] respectively
h = parameter in Eq. 32
k = wave number, m^{-1}
k_{min}, k_{max} = wave numbers of the largest eddy(e.g., D_{im}) and the smallest eddy existing in the flow, respectively, m^{-1}
l = parameter in Eq. 32
$m(V_0)$ = mean number of daughter droplets
$Ni(t)$ = number of droplets per unit volume of physical space in the ith size group at a given time t, m^{-3}
N_{im} = rotational speed of impeller, rpm (rev min^{-1})
n_d = number density of droplets per unit dispersion volume, m^{-3}
n_k = number density of eddies of wave number between k and $k+$dk, m^{-2}
$n(V, t)$ = number of droplets of volume V per unit volume of physical space per unit droplet volume at a given time t, m^{-6}
$n\lambda$ = number density of eddies of size between λ and $\lambda+d\lambda$, m^{-4}
Oh = Ohnesorge number ($=\mu_d/(\rho_d d_0 \sigma)^{1/2}$)
$P(k, a, b)$ = probability for droplet to break into n daughter droplets when an droplet of semiaxses a and b interacts with an eddy of wave number k

$P(k, d_0)$ = probability for droplet to break into n daughter droplets when a droplet of equivalent size d_0 interacts with an eddy of wave number k
r = distance from the centroid of eddy, m
r_0 = radius of droplet, m
S = surface area of a droplet, m^2
S_{ab} = collision cross-sectional area between an droplet with semiaxses a and b and an eddy of wave number k, m^2
S_d = shape factor
t = time, s
T = period of surface oscillation of a droplet, s
u = velocity in a turbulent eddy, m s^{-1}
u_c = critical eddy velocity required for fluid particle breakage, m s^{-1}
u_e = eddy velocity, m s^{-1}
uk = velocity of an eddy of wave number k, m s^{-1}
$u\lambda$ = velocity of an eddy of size λ, m s^{-1}
$\bar{u}$ = mean velocity at a distance of d_0 in an eddy, m s^{-1}
$\bar{u}(d_0)$ = mean velocity fluctuation of the underlying fluid at a distance of d_0, m s^{-1}
$\bar{u}k$ = mean velocity of eddy of wave number k, m s^{-1}
$\bar{u}_s$ = mean characteristic velocity of surface oscillation, m s^{-1}
$\bar{u}\lambda$ = mean velocity of eddy of size λ, m s^{-1}
V = volume of droplet, m^3
Vi = volume of daughter droplet, m^3
V_0 = volume of parent droplet, m^3
V_{min} = minimal volume of droplet, m^3
X = distance from the initial position of the surface, m
$y(t)$ = dimensionless variable (=$y'(t)/r_0$)
$y'(t)$ = distance from the initial position of mass center of half droplet, m

Greek letters

α_d = volume fraction of dispersed phase
β_1, β_2 = coefficients
βi = breakage rate defined by Prince and Blanch,[11] s
$\beta(f_v, V_0)$ = volume-based DSD probability density of forming droplets sizes of f_vV_0 and other daughter droplets
$\beta n(f_d, d_0)$ = DSD probability density of forming n daughter droplet (n=2, 3, 4) where at least one of the size fractions of daughter droplets equals to f_d
ε = turbulent dissipation rate per unit mass, m^2 s^{-3}
ε_d = turbulent dissipation rate per unit mass in the discharge flow region, m^2 s^{-3}
εi = turbulent energy dissipation rate per unit mass of impeller region, m^2 s^{-3}
εm = mean turbulent dissipation rate per unit mass over the whole stirred tank, m^2 s^{-3}
η = Kolmogorov scale, m
θ_{min} = product of *kmin* and Kolmogorov scale
λ = eddy size, m
λ_e = average size of energy-containing eddies, m
λ_{min}, λ_{max} = minimal and maximal eddy size, respectively, m
μ_c = viscosity of continuous phase, Pa s
μ_d = viscosity of dispersed phase, Pa s
ν = kinematic viscosity, m^2 s^{-1}
ρ_c = density of continuous phase, Pa s
ρ_d = density of dispersed phase, Pa s
σ = surface tension, N m^{-1}
ϑ = dimensionless energy
$\vartheta_{c,n}$ = critical dimensionless energy required for the breakage of forming n daughter droplets
$\bar{\delta}$ = mean amplitude of surface oscillation, m
τ_e = characteristic time of eddy of wave number k, s^{-1}
ϕn = breakage frequency density of a droplet of size d_0 breaking into n daughter droplets (n=2, 3, 4) with a given f_v, m^{-3} s^{-1}
$\varphi n(f_v,V_0)$ = partial breakage frequency density of a droplet of volume V_0 breaks into n daughter droplets where at least one of the daughters volumes equals to f_vV_0 (n=2, 3, 4), m^{-3} s^{-1}
$\psi(f_v,V_0)$ = overall partial breakage density of a droplet of volume V_0 of a given size fraction f_v, m^{-3} s^{-1}
$\Omega(V_0)$ = overall breakage frequency density of droplet of volume V_0, m^{-3} s^{-1}
$\Omega n(V_0)$, $\Omega n(a, b)$ = overall breakage frequency density of droplet of volume V_0 or an ellipsoidal droplet with semiaxses a and b breaking into n daughter droplets (n=2, 3, 4), m^{-3} s^{-1}
$\varpi(k, d_0)$ = frequency density of eddies of wave number k and $k+dk$ and droplets of size d_0, m^{-2} s^{-1}
$\varpi_{collision}(k, d_0)$ = collision frequency density of eddies of wave number k and $k+dk$ and droplets of size d_0, m^{-2} s^{-1}
$\varpi_{interaction}(k, d_0)$ = interaction frequency density of eddies of wave number k and $k+dk$ and droplets of size d_0, m^{-2} s^{-1}
$\varpi^*_{collision}(k, d_0)$ = specific collision density of eddies of wave number k and $k+dk$ and droplets of size d_0 (=$\varpi_{collision}(k, d_0)/[(1-\alpha_d)n_d]$), m s^{-1}
$\varpi^*_{interaction}(k, d_0)$ = specific interaction density of eddies of wave number k and $k+dk$ and droplets of size d_0 (=$\varpi_{interaction}(k, d_0)/[(1-\alpha_d)n_d]$), m s^{-1}

Literature Cited

1. Lasheras JC, Eastwood C, Martínez-Bazán C, Montañés JL. A review of statistical models for the break up of an immiscible fluid immersed into a fully developed turbulent flow. *Int J of Multiphase Flow*. 2002;28(2):247–278.
2. Jakobsen HA. Chemical Reactor Modeling: Multiphase Reactive Flows. Berlin: Springer-Verlag Berlin and Heidelberg GmbH & Co. KG, 2008.
3. Liao YX, Lucas D. A literature review of theoretical models for drop and bubble breakup in turbulent dispersions. *Chem Eng Sci*. 2009;64:3389–2406.
4. Marchetti JM, Svendsen HF. Review of Kernels for droplet-droplet interaction, droplet-wall collision, entrainment, re-entrainment, and breakage. *Chem Eng Commun*. 2012;199(4):551–575.
5. Solsvik J, Tangen S, Jakobsen HA. On the constitutive equations for fluid particle breakage. *Rev Chem Eng*. 2013;29(5):241–356.
6. Zainal Abidin MII, Abdul Raman AA, Mohamad Nor MI. Mean drop size correlations and population balance models for liquid—liquid dispersion. *AIChE J*. 2015;61(4):1129–1145.
7. Coulaloglou CA, Tavlarides LL. Description of interaction processes in agitated liquid-liquid dispersions. *Chem Eng Sci*. 1977;32:1289–1297.
8. Tsouris C, Tavlarides L. Breakage and coalescence models for drops in turbulent dispersions. *AIChE J*. 1994;40:395–406.
9. Chen Z, Prüss J, Warnecke HJ. A population balance model for disperse systems: drop size distribution *in emulsion*. *Chem Eng Sci*. 1998;53(5):1059–1066.
10. Maaβ S, Kraume M. Determination of breakage rates using single drop experiments. *Chem Eng Sci*. 2012; 70:146–164.
11. Prince MJ, Blanch HW. Bubble coalescence and breakup in air-sparged bubble column. *AIChE J*. 1990;36(10):1485–1499.
12. Martínez-Bazán C, Montañés JL, Lasheras JC. On the breakup of an air bubble injected into a fully developed turbulent flow. Part 1. Breakup frequency. *J Fluid Mech*. 1999;401:157–182.
13. Martínez-Bazán C, Montañés JL, Lasheras JC. On the breakup of an air bubble injected into a fully developed turbulent flow. Part 2. Size PDF of the resulting daughter bubbles. *J Fluid Mech*. 1999;401:183–207.
14. Luo H, Svendsen HF. Theoretical model for drop and bubble breakup in turbulent dispersions. *AIChE J*. 1996;42(5):1225–1233.
15. Lehr F, Mewes D. A transport equation for the interfacial area density applied to bubble column. *Chem Eng Sci*. 2001;56:1159–1166.
16. Lehr F, Millies M, Mewes D. Bubble-size distributions and flow fields in bubble columns. *AIChE J*. 2002;48:2426–2443.
17. Wang TF, Wang JF, Jin Y. A novel theoretical breakup kernel function for bubbles/droplets in a turbulent flow. *Chem Eng Sci*. 2003; 58:4629–4637.
18. Xing CT, Wang TF, Guo KY, Wang JF. A unified theoretical model for breakup of bubbles and droplets in turbulent flows. *AIChE J*. 2015;61(4):1391–1403.
19. Zhao H, Ge W. A theoretical bubble breakup model for slurry beds or three-phase fluidized beds under high pressure. *Chem Eng Sci*. 2007;62:109–115.
20. Hagesaether L, Jakobsen HA, Svendsen HF. A model for turbulent binary breakup of dispersed fluid particles. *Chem Eng Sci*. 2002;57: 3251–3267.
21. Andersson R, Andersson B. On the breakup of fluid particles in turbulent flows. *AIChE J*. 2006;52:2020–2030.

22. Zaccone A, Gäler A, Maaß S, Kraume M. Drop breakage in liquid–liquid stirred dispersions: modelling of single drop breakage. *Chem Eng Sci*. 2007;62:6297–6307.
23. Konno M, Aoki M, Saito S. Scale effect on breakup process in liquid-liquid agitated tanks. *J Chem Eng Jpn*. 1982;16(4):312–319.
24. Eastwood CD. The Breakup of Immiscible Fluids in Turbulent Flows, PhD Thesis. San Diego: University of California, 2002.
25. Galinat S, Masbernat O, Guiraud P, Dalmazzone C. Drop break-up in turbulent pipe flow downstream of a restriction. *Chem Eng Sci*. 2005;60:6511–6528.
26. Han LC, Gong SG, Li YQ, Ai QH, Luo HA, Liu ZF, Liu YJ. A novel theoretical model of breakage rate and daughter size distribution for droplet in turbulent flows. *Chem Eng Sci*. 2013;102:186–199.
27. Hill PJ, Ng KM. Statistics of multiple particle breakage. *AIChE J*. 1996;42:1600–1611.
28. Diemer RB, Olson JH. A moment methodology for coagulation and breakage problems. Part 3-generalized daughter distribution function. *Chem Eng Sci*. 2002;57:4187–4198.
29. Risso F, Fabre J. Oscillations and breakup of bubble immersed in turbulent field. *J Fluid Mech*. 1988;372:323–355.
30. Han LC, Luo HA, Liu YJ. A theoretical model for droplet breakup in turbulent dispersions. *Chem Eng Sci*. 2011;66(4):766–776.
31. Lamont JC, Scott DS. An eddy cell model of mass transfer into the surface of a turbulent liquid. *AIChE J*. 1970;16(4):513–519.
32. Luk S, Lee YH. Mass transfer in eddies close to air-water interface. *AIChE J*. 1986;32(9):1546–1554.
33. Pope SB. Turbulent Flows. Cambridge: Cambridge University Press, 2000.
34. Ishihara T, Gotoh T, Kaneda Y. Study of high-Reynolds number isotropic turbulence by direct numerical simulation. *Annu Rev Fluid Mech*. 2009;41:165–180.
35. Hinze JO. Turbulence. New York: McGraw-Hill, 1975.
36. Panchev S, Kesich D. Energy spectrum of isotropic turbulence at large wavenumbers. *C R Acad Bulg Sci*. 1969;22:627–630.
37. Von-Karman T. Progress in statistical theory of turbulence. *Proc Natl Acad Sci USA*. 1948;116:43–52.
38. Gotoh T, Fukayama D. Pressure spectrum in homogeneous turbulence. *Phys Rev Lett*. 2001;86:3775–3778.
39. Gotoh T, Fukayama D, Nakano T. Velocity field statistics in homogeneous steady turbulence obtained using a high-resolution direct numerical simulation. *Phys Fluids*. 2002;14:1065–1081.
40. Sreenivasan KR. On the universality of the Kolmogorov constant. *Phys Fluids*. 1995;7:2778–2784.
41. Liepmann HW, Robinson MS. Counting methods and equipment for mean value measurements in turbulence research, Technical Report No. 3037. Washington DC: National Advisory Committee for Aeronautics, 1953.
42. Kresta SM, Wood PE. The flow field produced by a pitched blade turbine: characterization of the turbulence and estimation of the dissipation rate. *Chem Eng Sci*. 1993;48(10):1761–1774.
43. McManamey WJ, Davies JT, Woollen JM, Coe JR. The influence of molecular diffusion on mass transfer between turbulent liquids. *Chem Eng Sci*. 1973;28(4):1061–1069.
44. Han LC, Gong SG, Li YQ, Gao NN, Fu J, Luo HA, Liu ZF. Influence of energy spectrum distribution on drop breakage in turbulent flows. *Chem Eng Sci*. 2014;117:55–70.
45. Ghasempour F, Andersson R, Andersson B, Bergstrom DJ. Number density of turbulent vortices in the entire energy spectrum. *AIChE J*. 2014;60(11):3989–3995.
46. Clark MM. Drop breakup in a turbulent flow-I. Conceptual and modeling considerations. *Chem Eng Sci*. 1987;43(3):671–679.
47. Andersson R, Andersson B. Modeling the breakup of fluid particles in turbulent flows. *AIChE J*. 2006;52:2031–2038.
48. Nambiar DKR, Kumar R, Das TR, Gandhi KS. A new model for the breakage frequency of drops in turbulent stirred dispersions. *Chem Eng Sci*. 1992;47(12):1989–3002.
49. Han LC, Luo HA, Liu YJ, You KY, Liu PL. A multi-scale theoretical model for gas-liquid interface mass transfer based on the wide spectrum eddy contact concept. *AIChE J*. 2011;57(4):886–896.
50. Maaß S, Buscher S, Hermann S, Kraume M. Analysis of particle strain in stirred bioreactors by drop breakage investigations. *Biotechnol J*. 2011;6(8):979–992.
51. Escudié R, Liné A. Experimental analysis of hydrodynamics in a radially agitated tank. *AIChE J*. 2003;49(3):585–603.
52. Baldi S, Yianneskis M. On the quantification of energy dissipation in the impeller stream of a stirred vessel from fluctuating velocity gradient measurements. *Chem Eng Sci*. 2004;59:2659–2671.
53. Kumar S, Ramkrishna D. On the solution of population balance equations by discretization–I: a fixed pivot technique. *Chem Eng Sci*. 1997;51(8):1311–1332.
54. Placek J, Tavlarides LL. Turbulentflow in stirred tanks. Part I: turbulent flow in the turbine impeller region. *AIChE J*. 1985;31:11–13.

Manuscript received Nov. 4, 2014, and revision received Feb. 16, 2015.